Inclusive (p,α) and $(p,^3He)$ cross sections induced by 100 MeV protons on ^{40}Ca

Tshifhiwa Moureen Masikhwa

Thesis presented in fulfillment of the requirements for the degree of Master of Sciences at the University of the Western Cape.

Supervisor: Dr S.V. Förtsch

Physics Group

iThemba LABS

Co-supervisor: Prof R.Lindasy

Physics Group

University of the Western Cape

April 2006

Keywords

- Prescaled singles
- Continuum Spectra
- Complex particle emission
- Particle Identification (PID)
- Double differential cross sections
- Quasifree knockout
- Multistep direct
- Exciton Model

DECLARATION

I, the undersigned, hereby declare that the work contained in this thesis is my own original work and that I have not previously in its entirety or in part submitted it at any university for a degree.

Signature: ..MASIKHWA T.M.....

Date: ....15-03-07.....

Inclusive (p,α) and $(p, {}^3He)$ cross sections induced by 100 MeV protons on ^{40}Ca

Tshifhiwa Moureen Masikhwa
iThemba LABS, old Faure Road, Somerset West 7129, South Africa
e-mail: masikhwa@tlabs.ac.za

ABSTRACT

Alpha clustering in nuclei is studied with quasi-free knockout reactions. A beam of 100 MeV polarized protons was used in the quasi-free knockout reaction $^{40}Ca(\vec{p},p'\alpha)^{36}Ar$ at iThemba LABS. While the scattered protons were detected in the K600 magnetic spectrometer, the alpha particles were measured with a detector telescope consisting of three silicon surface barrier detectors. Both coincidence and pre-scaled singles events were recorded to extract cross sections as well as analyzing powers. The inclusive spectra of $^{40}Ca(p,\alpha)$ and $^{40}Ca(p,^3He)$ were extracted from the prescaled-singles data. The prescaled single events were analyzed in order to test the efficiency of the silicon detector telescope and to obtain the double differential cross sections of the emitted ^{3}He and ^{4}He particles. Results of the experimental cross section spectra were compared to calculated angular distributions based on the Kalbach systematics as well as the preequilibrium exciton model code PRECO-2000. Both this model as well as the phenomenological prescription are able to reproduce reasonably well the inclusive energy spectra of the emitted ^{3}He and ^{4}He particles. This leads to the conclusion that the reaction mechanism is governed by a multistep mechanism leading to the emission of ^{3}He and ^{4}He as clusters of excited nucleons from the composite nucleus.

Cross Sections dzo katelaho dza (p,α) na (p,^{3}He) dzo bveledzwa kha ^{40}Ca nga protons dza 100 MeV

Tshifhiwa Moureen Masikhwa
iThemba LABS, old Faure Road, Somerset West 7129, South Africa
e-mail: masikhwa@tlabs.ac.za

MANWELEDZO

Kuvhangano ya alpha nga ngomu ha nuclei inga gudwa hu tshi shumiswa vhutanganyi ha *knockout*. Ho shumiswa *beam* ya *protons* dza 100 MeV dzo sumbaho huthihi kha vhutanganyi ha *knockout* ho vholowaho lwa mafanedza ha ^{40}Ca $(p, p\alpha)^{36}$Ar ngei iThemba LABS. Naho *protons* dzo phadalaho dzo vhonwa kha *Spectrometer* tsha maginethe tsha K600, zwipida zwa alpha zwo kalwa nga *detector* ivhonelaho kule yo fhatwaho nga *detector* tharu dzo tsireledzwaho nga luvhemba lwa *Silicon*. Ho wanala zwithu zwo bvelelaho mazha khathihi na zwo thomaho zwaela zwa kona u bvelela nga tshithihi-tshithihi. Zwi-*spectra* zwo katelaho zwa $^{40}Ca(p,\alpha)$ na zwa $^{40}Ca(p,^3He)$ zwo nulwa zwi tshi bva kha zwidodombedzwa-vhuthihi zwo thomaho zwa kalwa. Ho senguluswa zwidodombedzwa vhithihi zwo kalwaho u thoma hutshi itelwa u linga vhukoni ha *detector* ya *Silicon* ivhonelaho kule khathihi nau wana dzi *differentoal cross sections* kavhili dza zwipida zwo bveledzwaho zwa ^{3}He na ^{4}He. Mvelelo dza experiment dza zwi-*spectra* zwa cross sections dzo do vhambedzwa na u thalangana ha dzi-engele dze dza tou tanganyelwa hu tshi khou shumiswa kuitele kwa *Kalbach* khathihi na tshifanyiso tsha *exciton* tsha khoudu ya *PRECO-2000*. Tshifanyiso isthi khathihi na muthetho u pfesessaho zwi a kona u bvisa nga ndila ipfadzaho zwi-*spectra* zwo bveledzwaho zwa ^{3}He na ^{4}He. Mvelelo idzi dzi khou wanala dzi tshi andana na kuitele kwa *Kalbach* khathihi na tshifanyiso tsha *exciton* tsha khoudu ya *preequilibrium PRECO-2000*.

ACKNOWLEDGEMENTS

I wish to express my sincere gratitude to my University supervisor, Prof R.Lindsay, and my co-supervisor, Dr.S.V. Förtsch for their excellent advice and invaluable supervision towards my studies.

I would also like to thank:

- N.T. Botha, E.Z. Buthelezi, A. Cowley, H. Fujita, G.C. Hillhouse, T.E. Lakaje, R. Neveling, S Ntshangase, L.J. Mudau, F.D. Smit, D.F. Steyn, J. Van der Merwe, B. Van der Ventel, D Van Niekel, and S. Wyngaardt, for their many hours of data taking.

- The invaluable assistance received from Dr. R. Neveling, who was never too busy to help.

- The MANUS/MATSCI co-ordinators, C. Theron, Profs O.M. Ndwandwe and Profs J.F. Sharpe-Schafer for making that everything possible.

- J. Mudau, N. Botha and T. Lakaje, for their assistance and moral support.

- Koni Rashamuse for being there and providing much needed encouragement and unconditional support during my difficult time.

- My colleagues MANUS/MATSCI students and all my friends for their cooperation and support.

- I am grateful to iThemba LABS and the NRF, for their financial support.

- All staff and postgraduate within the iThemba Physics Group.

- I am deeply appreciative of the support, love and encouragement I have received from my mother, for the faith which she has always maintained in my ability, showing me that life is a precious gift from God and that with God everything is possible. I am who I am because of the love and sacrifices she made for me.

- I am also grateful to my family, Mr.R.Maluleke, Mrs.D.E.Maluleke, Mr. M.B.Masikhwa and Mr.T.M.Masikhwa for their support, love and encouragement throughout my studies. I owe them so much, making it difficult to express my sincerest gratitude.

- Thank God, The Almighty for granting me, gives me guidance and serenity to take such a challenging and demanding task.

I dedicate my special thanks to the late Dr.T.K.Marais for all the things that he had done for me and giving me break to further my studies.

CONTENTS

LIST OF FIGURES

LIST OF TABLES

CHAPTER 1 INTRODUCTION

In this chapter an introduction to the continuum scattering of complex particles at incident energy of 100 MeV on ^{40}Ca target is given. This is followed by a short description of previous work that was done involving the double differential cross sections. Inclusive reactions, statistical multistep reactions and the aim of the study are also described.

1.1 α-Clustering

Clustering is defined as the formation of a small group of nucleons inside the nucleus that move together. ^{3}He and ^{4}He particles are often referred to as preformed clusters inside the nucleus. Of all possible clusters the alpha particle is the most stable due to its high symmetry and binding energy [Hod93]. Hence clustering in nuclei is mainly restricted to alpha particle clustering. The bound α-cluster wave function $\phi^{\alpha}_{L\Lambda}$ used for instance in distorted wave born approximation calculations can be taken to be eigenstates of an α-particle separation energy [Nad99]. The quantum numbers N were chosen to be those corresponding to a harmonic-oscillator shell model. As an example for 1p-shell nuclei the quantum number is 3S for L=0 transitions and 2D for L=2 transions [Nad99] and assuming $(1s^4)$ $(1p^{12})$ $(2s1d)^4$ configurations for ^{20}Ne, L=0(2) transitions must have N=3(2) [Wang80]. Alpha clustering has found many applications in nuclear reactions and nuclear structure [Hod93]. Nuclear structure calculations show that alpha clustering is more likely to take place at the nuclear surface where the density is lower, and this would indicate that light nuclei have a cluster structure. The existence of an alpha particle near the surface could result in the escape of alpha particles. Another proof of the existence of alpha particles in the nuclear surface is the development of reactions involving the removal or capture of an alpha particle [Hod93]. The study of alpha transfer reactions allows the alpha particle bound and unbound states of nuclei to be found [Hod93]. There are different ways of investigating clustering both theoretically as well as experimentally. These are through pickup, stripping and quasi-free knockout reactions.

Alpha clustering in light nuclei, specifically ^{6}Li, ^{7}Li, ^{9}Be and ^{12}C, has been extensively studied by means of $(p, p\alpha)$ quasi-free knockout reaction at energies between 100 MeV and 296 MeV [Roo77, Nad80, Wan85, Nad89, Yosh98]. Based on the good shape agreement between the distorted wave impulse approximation (DWIA) calculations and the experimental energy sharing differential cross section data from these studies, it was concluded that the reaction is largely a quasifree process and that the distorted wave impulse approximation provides an appropriate description of the reaction.

Cluster knockout was also studied with the $(\alpha,2\alpha)$ reaction on ^{9}Be and ^{12}C at incident energy of 580 MeV [Nad99]. Each energy sharing distribution is characterized by a smooth broad distribution reaching a maximum near the energy corresponding to zero recoil momentum of the residual nucleus, indicating a dominance of quasi-free alpha knockout. A comparison of the ^{9}Be and ^{12}C data for the same alpha particle angles shows that the peak cross sections for ^{12}C are roughly a factor of 5 smaller than those for ^{9}Be [Nad99]. The data were compared with the DWIA calculations. It was found that the theory and the experiment suggest a dominance of the quasifree knockout mechanism.

The $(\alpha,2\alpha)$ reaction is a reliable tool for extracting alpha cluster spectroscopic information from light nuclei at incident energies of 200 MeV and above [Stey99, Nad99]. DWIA analysis of proton induced alpha cluster knockout from light nuclei yield consistent spectroscopic factors over the whole studied energy range from 100 to 296 MeV. Proton induced alpha cluster knockout thus seems to be superior to transfer reactions and alpha induced cluster knockout reactions in providing absolute alpha particle spectroscopic factor [Wan85], and thus information about clustering in the nuclei.

The $(p, p'\alpha)$ quasifree knockout cross sections were supplemented by analyzing powers (A_y) which were measured under the same experimental conditions. These analyzing powers were found to act as a more stringent test of the reaction dynamics, which consequently influence conclusions drawn about the cluster structure of the studied nuclei. The data for such measurements are limited. Wang *et al.* [Wan85]

report that for the $^{9}Be(\vec{p}, p\alpha)$ reaction at 150 MeV the energy sharing analyzing power distribution agrees reasonably well with the theoretical calculations. Similarly Yoshimura *et al.* [Yosh98] found that energy sharing analyzing power distributions are reproduced fairly well for the $(p, p\alpha)$ reaction at 296 MeV for the targets ^{6}Li, ^{7}Li and ^{9}Be. This confirms that the reaction is largely a quasifree process and that there is little contribution from a multistep process. However, in contrast to the findings based on the cross section alone, the significant differences between the experimental analyzing power and the DWIA calculations for the $^{12}C(\vec{p}, p\alpha)$ reaction at 296 MeV [Yosh98] indicate significant contributions from processes other than the quasi-free knockout reaction.

Little effort has thus far gone into the investigation of alpha particle clustering in heavier nuclei by means of proton induced quasi-free cluster knockout reactions. Only cross section data are available at an incident energy of 100 MeV. Carey *et al* [Car84] investigated the ground state $(\vec{p}, p\alpha)$ reaction at quasi-free kinematics with a range of target nuclei heavier than ^{12}C (^{16}O, ^{20}Ne, ^{24}Mg, ^{28}Si, ^{40}Ca, ^{48}Ti, ^{54}Fe and ^{66}Zn) at 101.5 MeV. Nadasen *et al.* [Nad81] studied the non-coplanar $^{40}Ca(\vec{p}, p\alpha)$ reaction at 101.3 MeV in order to access higher momentum components of the cluster wavefunction. For both these studies DWIA calculations agree with the experimental energy sharing cross section distributions.

The reason for carrying out the present study on ^{40}Ca target was based on the fact that the probability of alpha cluster formation is at maximum for mass=40 at 101.5 MeV [Car84]. It is expected that, if the quasi-free knockout reaction mechanism represents a good approximation of the reaction, the analyzing power where the residual nucleus has zero recoil momentum, should approximately correspond to free *p-α* elastic scattering data. This was illustrated by Wang *et al.* [Wan85] for the ^{9}Be $(p, p\alpha)$ reaction at 150 MeV as shown in figure 1.1

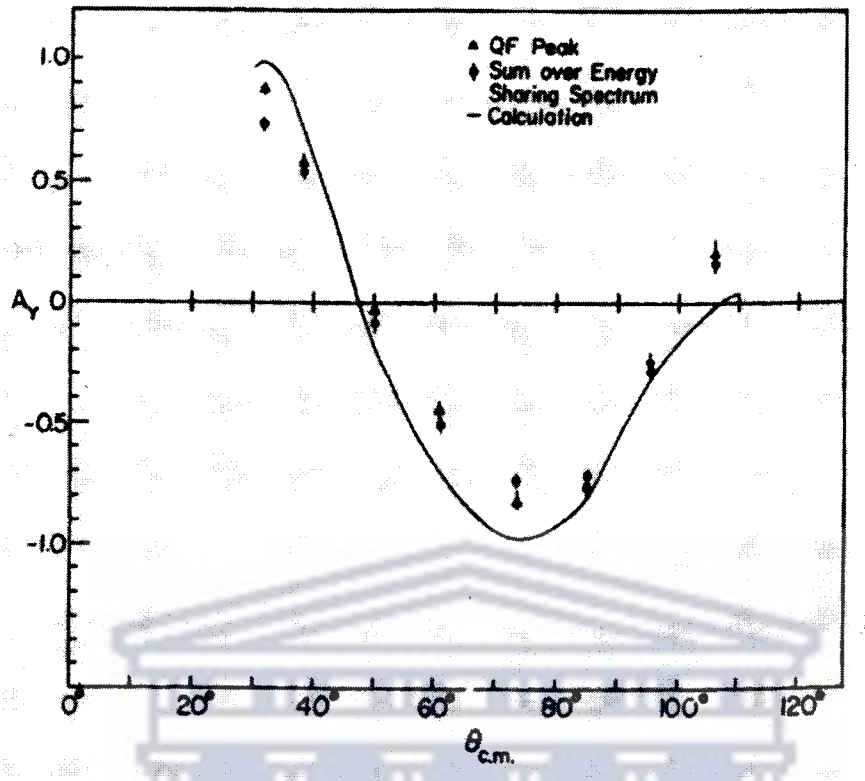

Figure 1. 1: *$^{9}Be(\vec{p}, p\alpha)^{5}He$ analyzing power data at the quasifree peak (triangles) as a function of the two-body center of mass $p-\alpha$ scattering angle for an incident proton beam of 150 MeV [Wan85]. The circles represent A_y summed over the full energy sharing distribution. The curve represents free $p-\alpha$ data.*

1.2 Inclusive spectra

The measurements of inclusive reactions include all reaction channels over the full excitation energy range, while exclusive measurements restrict themselves to a specific excitation region as well as phase space. The energy spectra of charged particles emitted in the interaction of medium energy protons with nuclei are characterized by three different regions. A typical inclusive energy spectrum of particles emitted from nuclear reactions is shown in figure 1.2. At the upper end of the spectrum are a number of discrete states due to elastic scattering and low excitations of the target nucleus. At low emission energy the evaporation peak (Equilibrium) can

be seen. Evaporation of nucleons occurs when the incident energy is shared among the nucleons of the target nucleus. Once this equilibration process has taken place the average energy per nucleon is below the binding energy and the compound nucleus can exist in excited states over relatively long periods. The de-excitation will occur when a single nucleon or group of nucleons acquire enough energy to escape. The compound nucleus therefore loses its energy or cools down by evaporating nucleons and clusters. Between these two extreme regions in the energy spectrum the so called broad "continuum" appears. In these reactions the projectile and target interact by successive nucleon-nucleon collisions. The incident energy is thereby shared among nucleons, leaving at least one particle in the continuum.

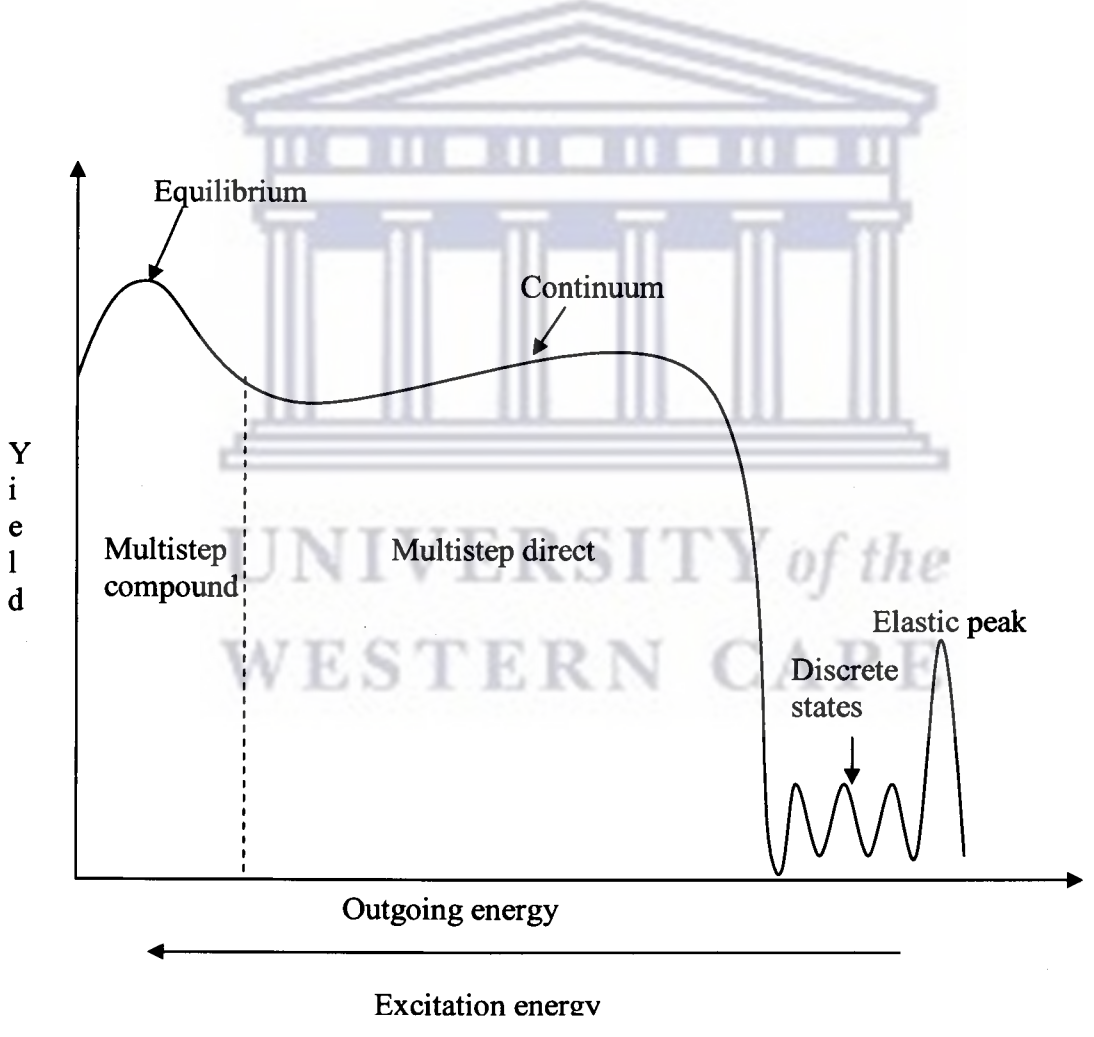

Figure 1.2: *Energy spectrum of particles emitted from nuclear reactions*

Cross sections for the inclusive *(p,α)* and *(p,^{3}He)* reaction on ^{12}C, ^{27}Al, ^{58}Ni, ^{90}Zr and ^{209}Bi using 72 MeV polarized protons in the angular range of 10^0 up to 145^0 were investigated by Lewandowski *et al.* [Lew82]. The shapes of the differential cross sections for the *(p,α)* and *(p,^{3}He)* reactions are very similar and are essentially independent of the target nucleus mass number. The cross sections of the $(\vec{p},^3He)$ reactions is about ten times smaller than of the $(\vec{p},\alpha)$ reaction. The results of the $^{27}\mathrm{Al}(\vec{p},\alpha)$, $^{90}\mathrm{Zr}(\vec{p},\alpha)$ as well as for the ^{58}Ni $(\vec{p},^3He)$ reaction were compared with the multistep direct reaction model of Tamura *et al.* [Tam81]. The experimental results agree with the theoretical calculations showing that the theory can be applied successfully for describing cross sections [Lew82]. It was found that the reaction mechanism for the emission of ^{4}He can be linked to quasifree knockout whereas for ^{3}He emission it is deuteron pickup mechanism linked to a multistep process described by a chain of nucleon-nucleon interactions inside the composite nucleus..

Continuum cross sections as well as continuum analyzing powers for the inclusive $(\vec{p},^3He)$ reaction on ^{59}Co and ^{93}Nb at an incident energy of 100 MeV were investigated by Cowley et al [Cow00]. The results show that at 90 MeV, which is approximately the highest outgoing ^{3}He energy, the continuum cross sections and analyzing powers are well reproduced by the first step of a multistep pickup process [Cow00]. For lower outgoing energies the two-step and three-step processes contribute increasingly to the cross sections and analyzing powers. The results were compared with the multistep direct theory of Feshbach, Kerman and Koonin (FKK) [Fes80] assuming that the reaction mechanism is deuteron pickup linked to a multistep direct mechanism. The analyzing powers prove to be a sensitive measure of the contribution of the various one step and multistep processes [Cow00].

Analyzing powers of the $^{58}Ni(\vec{p},\alpha)$ reaction at E_p=22 and 72 MeV measured for transitions to the ground state of ^{55}Co as well as to excited states in the continuum, were investigated by Bonetti *et al.* [Bon89]. For transition to the ground state the analyzing powers were calculated with the distorted wave Born approximation (DWBA) using an alpha knockout and a triton pickup mechanism. The DWBA calculations were done with the help of the DWUCK5 [Kun] and TWOFNR [Iga] codes for triton pickup as well as alpha knockout processes, respectively. The

analyzing powers at 72 MeV in the continuum were calculated with the statistical multistep direct theory of Feshbach, Kerman and Koonin (FKK) [Fes80]. It was found that while the ground state transition is dominated by the triton pickup process, the analyzing power in the continuum can only be reproduced by an alpha knockout mechanism as the final step.

Continuum analyzing powers were measured for 65 MeV protons for ^{93}Nb$(\vec{p},\alpha x)$ and ^{209}Bi$(\vec{p},\alpha x)$ reactions [Sak80]. At the excitation energy above 10 MeV the analyzing powers are non-zero and vary smoothly with excitation energy. The analyzing powers are small at forward angles where the preequilibrium process is important [Sak80]. The analyzing powers are large and positive at backward angle where the shape of the continuum spectra resemble those of evaporation spectra. The results were compared with the multistep direct reaction model of Tamura *et al.* [Tam81] where the continuum energy spectra of $(\vec{p},\alpha)$ reactions were reproduced successfully. It was found that the measurements of the continuum analyzing powers could be interpreted successfully by the multistep direct reaction model of Tamura *et al.* [Tam81].

At higher incident energies Green *et al.* [Gr82] investigated ^{3}He and ^{4}He emission at angles of 60^{0} and larger in bombardments of a ^{nat}Ag target with polarized protons with energies of 237, 445 and 518 MeV. It was concluded that the observed yield at higher energies could not be accounted for by a direct knockout mechanism. However, since the measurements of Green *et al.* [Gr82] were performed at relatively large angles the observed spectra may be dominated by equilibrated emission, for which a zero analyzing power would be expected. Renshaw *et al.* [Ren91] measured zero analyzing powers on $^{nat}Ag + \vec{p}$ at 200 MeV for a variety of ejectiles at 15^{0} with $Z \leq 7$. They concurred with the conclusions from the studies at even higher energies [Gr82] that a simple mechanism such as direct cluster knockout or a similar one step process can be excluded.

In an attempt to reconcile these two contrasting results, where on the one hand the reaction mechanism was found to correspond to a direct one step process whereas, on the other hand, such a mechanism was totally excluded, Cowley *et al.* [Cow96, Cow97] investigated the cross sections for the inclusive emission of ^{3}He and ^{4}He from

^{27}Al, ^{59}Co and ^{197}Au at incident energies of 120, 160 and 200 MeV. The results were compared with calculations based on the statistical multistep direct reaction theory of Feshbach, Kerman and Koonin (FKK) [Fes80]. It was found that the reaction mechanism for the emission of ^{3}He can be linked to deuteron pickup whereas a knockout mechanism as the final step dominates in the case of alpha particle emission.

Similarly, analyzing powers for the inclusive $(\vec{p},\alpha)$ reaction on ^{59}Co at an incident energy of 100 MeV were investigated [Cow02]. The experimental results were compared with a simple knockout model. It was found that the analyzing powers seem to be guided by the single step knockout interpretation at high alpha emission energies [Cow02]. The comparison between the experimental analyzing power for the inclusive $(\vec{p},\alpha)$ reaction on ^{59}Co at an incident energy of 100 MeV, and the results predicted by the simple knockout model suggest that a one step mechanism dominates the emission of alpha particles for small energy transfers [Cow02]. The results were also compared to the previous results obtained for the inclusive $(\vec{p},^{3}He)$ reaction on ^{59}Co and ^{93}Nb at an incident energy of 100 MeV [Cow02]. It was found that the single step mechanism appears to persist to higher excitation energies of the residual system for the $(\vec{p},\alpha)$ reaction than was previously found for the $(\vec{p},^{3}He)$ reaction.

1.3 Statistical Multistep Reactions

Two reaction mechanisms, which successfully describe compound nucleus as well as direct nuclear reactions, were used to analyse a large number of nuclear reactions. The bulk of the measured cross sections however indicates that these particles are emitted after the direct reactions but before the formation of a compound system. These reactions are commonly referred to as the preequilibrium reactions [Gad92]. At the excitation energies at which these reactions occur the excited states are very close to each other. Feshbach, Kerman and Koonin [Fes92] developed a statistical multistep [Fes92] theory that postulates two different statistical processes namely the multistep compound (MSC) and the multistep direct (MSD). In the MSC reactions all the

particles including the projectile as well as target nucleons remain bound during the equilibration cascade whereas in the MSD reactions the projectile remains in the continuum. Particle emissions take place after the direct and before the attainment of full statistical equilibrium. The multi-step compound and the multi-step direct reactions take place on very different time-scales. The multi-step direct processes take place in the time it takes the projectile to transverse the target nucleus which is in the order of 10^{-22} seconds whereas the multistep compound process takes much longer, about 10^{-15} seconds[Fes80].

Typical angular distributions of the differential cross sections in the centre of mass system of reaction products from direct and compound nuclear reactions are shown in figure 1.3. The direct reactions are characterized by the emission of medium to high–energy particles with the excitation of the lower energy states of the target nucleus, while for the compound reactions the emission of low-energy particles leave the residual nucleus in extremely high states [Gad92]. In the center of mass system the angular distribution of a compound reaction is symmetric about 90^0 while the angular distribution of a multi-step direct process is forward-peaked since the interaction is restricted mainly to peripheral collisions from which the emitted particles will carry most of the incident energy and momentum of the projectile [Gad92].

At incident energies of 100 to 200 MeV the statistical multistep model of Feshbach, Kerman and Koonin (FKK) [Fes80] has been used to analyse proton induced reactions such as (p,p')[Cow90], (p,α)[Cow96] and $(p,^3He)$[Cow97]. The statistical multistep theory of Feshbach, Kerman and Koonin (FKK) [Fes80] was used by Kalbach and Mann [Kal81] in their empirical parametrization of preequilibrium cross sections. These parameterizations are used as an approach to establish the role which the multistep direct (MSD) and multistep compound (MSC) processes play in these reactions. The distinction between the multistep compound and the multistep direct reactions was used by Kalbach and Mann in the empirical parametrization of pre-equilibrium reactions [Kal88].

Different theoretical approaches have predicted continuum emission consisting of a series of particle-hole excitations with creation probability of emission after each step.

The semi classical exciton model proposed by Griffin [Gr66] describes the reaction process in terms of a series of nucleon-nucleon interactions within the nucleus. The model assumes that the nucleus is excited by a series of nucleon-nucleon collisions between the incident projectile and the target nucleons. These take place in a series of stages, beginning with the projectile in the continuum. The first interaction excites the nucleons to a higher shell-model state creating a particle-hole pair. The second interaction creates a further particle-hole pair leading to a two-particles, one-hole (2p1h) state [Gad92]. Subsequent interactions create additional particle-hole pairs giving 3p2h states etc. This process continues until the incident energy is shared among the nucleons of the target nucleus [Gad92]. At each stage there is a possibility that one of the nucleons gains enough energy to escape from the composite nucleus. The process continues until the incident energy is spread through the nucleus. The exciton model was used to calculate the continuum complex particle emission for 90 MeV protons on ^{27}Al, ^{58}Ni, ^{90}Zr and ^{209}Bi and 100 MeV protons on ^{58}Ni [Wu79]. It was found that for heavy nuclei the preequilibrium reaction dominates the cross sections for complex particle emission.

The exciton model treat the process of the emission of ^{4}He can be linked to quasifree knockout whereas for ^{3}He emission is deuteron pickup mechanism linked to a multistep process describing a chain of nucleon-nucleon interactions inside the composite nucleus with the eventual emission of ^{3}He or ^{4}He particle to the continuum as the final step.

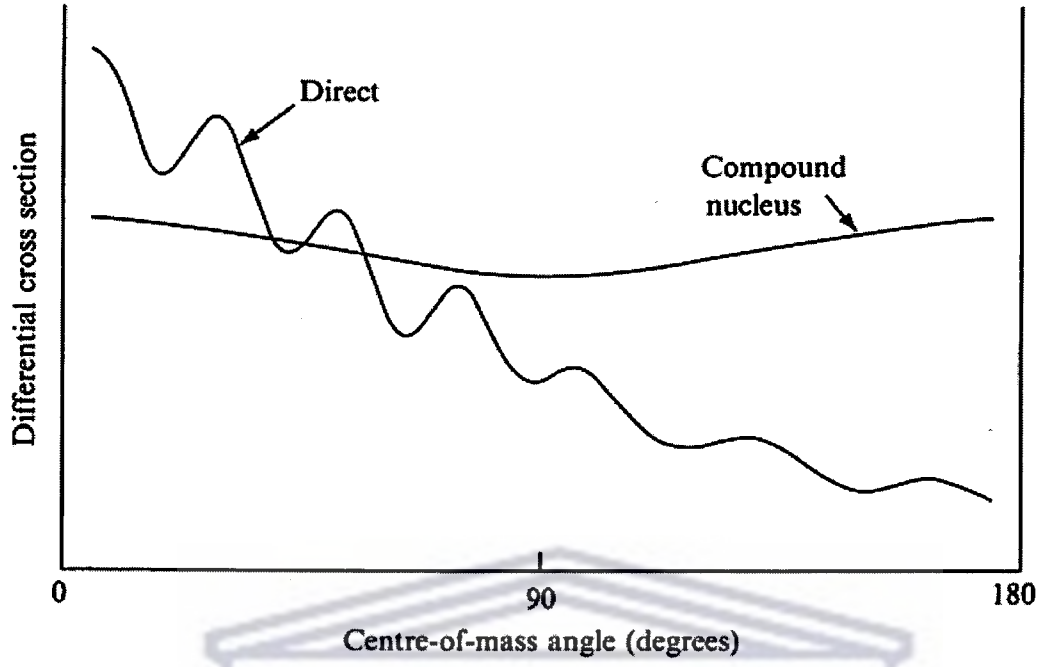

Figure 1.3*: Typical angular distributions for the differential cross section in the centre of mass system of reaction products from direct and compound nucleus reactions.*

1.4 Aims of this study

In the present study clustering of ^{3}He and ^{4}He in ^{40}Ca is investigated by means of proton-induced reactions. A beam of 100 MeV polarized protons was used to study the quasi-free knockout reaction $^{40}Ca(\vec{p},p'\alpha)^{36}Ar$. In this knockout reaction the incident proton collides with an α-cluster in the target and knocks it out. The reaction takes place at incident energies much higher than the binding energy of the knocked out particle. The incident proton beam knocks out the alpha particle, which is bound to the target ^{40}Ca to produce three reaction products, which are the scattered proton p′, knocked out alpha particle and the residual nucleus ^{36}Ar. The momentum of the incident projectile is shared between the knocked out particle and the scattered particle leaving the residual nucleus at zero momentum. This condition is referred to as quasi-free knockout.

Coincidence analyzing powers and double differential cross sections between the alpha particles and the scattered protons were measured at the quasifree angle pairs of $(\theta_{K600}, \theta_{telescope}) = (59^0, -51.5^0)$, $(70^0, -45.5^0)$ and $(81^0, -40.1^0)$. As part of the overall data analysis the present study had the following two aims: The first was to test the efficiency of the silicon detector telescope, which was used to detect the alpha particles. The second was to extract the double differential cross sections of the ^{3}He and ^{4}He emitted particles from the prescaled singles data set at the emission angles of 40.1^0, 45.5^0 and 51.5^0 and to test these against preequilibrium exciton model calculations.

In the present study exciton model and Kalbach systematics calculations were performed for the cross sections of the inclusive (p, α) and (p, ^{3}He) reactions on ^{40}Ca at an incident energy of 100 MeV at lab angles of 40.12^0 and 51.5^0. The preequilibrium exciton model and the Kalbach systematics are applied in the present study to determine whether these represent a reasonable interpretation of the basic physics underlying the interactions giving rise to the observed double differential cross sections.

In Chapter 2 the experimental setup and the electronics used for data acquisition are described. Chapter 3 is devoted to the analysis of the data and describe the procedure of data taking, while chapter 4 discusses the model calculations, which were compared with the data. In Chapter 5 the experimental and theoretical double differential cross sections of ^{4}He and ^{3}He are presented. The summary and conclusions are presented in Chapter 6.

CHAPTER 2 EXPERIMENT

2.1 Introduction

A beam of 100 MeV polarized protons was used to study the quasi-free knockout reaction $^{40}Ca(\vec{p},p'\alpha)^{36}Ar$. The experiment made use of two detectors in coincidence, namely the K600 magnetic spectrometer and a silicon detector telescope. The prescaled singles data which were measured with the silicon detector telescope, were analyzed in order to test the efficiency of the silicon detector telescope as well as to extract double differential cross sections of the inclusive spectra of the $^{40}Ca(p,\alpha)$ and $^{40}Ca(p,^{3}He)$ reactions. The experimental setup will be described in the following sections of this chapter.

2.2 Detector set-up

While the scattered protons were detected in the K600 magnetic spectrometer, the ^{3}He and alpha particles were measured with a detector telescope consisting of silicon surface barrier detectors. The different events that were measured and recorded during the experiment included coincidence, pre-scaled singles and pulser events. Coincidence events between the alpha particles and the scattered protons were measured at the quasifree angle pairs of (θ_{K600}, $\theta_{telescope}$) = (59^0, -51.5^0), (70^0, -45.5^0) and (81^0, -40.1^0). The minus sign for $\theta_{telescope}$ indicates an angle on the opposite side of the proton beam. The quasifree angle pairs were calculated using a three-body kinematics program. Three-body kinematics program provided the energies of the alphas and protons. Quasifree angle pairs with energy region of alpha and protons are shown in Table 2.1. The singles event rate in the silicon detectors and the K600 magnetic spectrometer were prescaled in order not to dominate the coincidence event rate.

Table 2. 1: *Quasifree angle pairs with the corresponding energy regions of the alphas and protons.*

Angle pairs	Proton energy range	Alpha energy range
$(59^0, -51.5^0)$	60-80 MeV	12-32 MeV
$(70^0, -45.5^0)$	54-74 MeV	19-39 MeV
$(81^0, -40.1^0)$	47-67 MeV	25-45 MeV

2.2.1 K600 Magnetic spectrometer

The scattered protons were measured at the focal plane of the K600 magnetic spectrometer, which was set at angles of 59^0, 70^0 and 81^0, respectively. The scattered protons enter the spectrometer through a collimator, which defines the solid angle of the spectrometer. A collimator of 63.2 mm in diameter was placed at the entrance of the spectrometer at a distance of 735.5mm from the target. The solid angle is calculated from the equation

$$\Delta\Omega = \frac{\pi r^2}{x^2}$$

where r=31.60 mm is the radius of the collimator and x = 735.50 mm is the distance from the target to the back of the collimator. The size of the solid angle was found to be 5.79 msr. The angular acceptance defined by the collimator is 4.92^0. The scattered proton then passes through a quadrupole and then through two dipole magnets. Protons with high energies will follow large radii while protons with low energies will follow small radii according to the equation

$$r = \frac{mv}{qB},$$

$r \equiv$radius of the scattered proton

$m \equiv$ mass of the scattered proton

$v \equiv$ velocity of the scattered proton

q ≡charge of the scattered proton and

B ≡magnetic field of the dipole magnet

where m, q and B are constant.

The vacuum pressure inside the spectrometer was of the order of 10^{-5}mbar. The exit window of the K600 is made of Kapton and is 80 cm long, 10 cm wide and 10 μm thick. Three drift chambers followed by two paddle plastic scintillation detectors are mounted at the focal plane of the spectrometer. The three-body kinematics program (Quasta) was used in order obtain the energy region of the detected protons where the momentum of the residual nucleus was zero.

Drift chambers

Drift chambers are used to determine the position of the scattered protons at the focal plane. The position gives energy information of the scattered protons. The drift chambers consist of two vertical drift chambers (VDCs) and one horizontal drift chamber (HDC). VDCs give information in the x- direction while HDC gives information in the y-direction. VDCs were used to determine the position information along the focal plane as well as the angle at which the scattered proton crossed the focal plane. Each vertical drift chamber consists of two aluminum cathode planes, which are made of 27 μm thick aluminum foils separated by a distance of 16mm. A voltage of –3 kV was applied to these Al planes. There are 200 vertical signal wires and 200 vertical guard wires between the aluminium cathode planes. The signal wires each 25 μm thick are spaced 4mm apart. The signal wires are at 0 V potential while the guard wires are at –500V. The guard wires provide field shaping and define cells associated with each signal wire of about 4mm. The guard wires each of thickness 50 μm are also spaced 4mm apart. The drift chambers are filled with 90% Ar and 10% CO_2. As a proton moves through the drift chamber it ionizes the gas. The electrons drift towards the signal wires, due to the potential difference between the wires and the aluminium planes. As an electron reaches a wire a signal is produced and sent via a preamplifier to a time-to-digital converter (TDC) with which the drift time of the electron is measured. In order to register a good event in each VDC at least three but not more than eight adjacent signal wires were needed to trigger. The focal plane

position is determined by using the drift times and wire position coordinates about three wires situated on either side of the wire associated with the lowest drift time. The horizontal drift chamber (HDC) has 16 wires and 17 guard wires respectively in the horizontal plane.

The plastic Scintillators

Two plastic scintillator paddles were mounted behind each other behind the drift chambers. Each paddle has a photomultiplier tube on either side. Since they have faster timing characteristics than the drift chambers they were used to define a K600 event whenever a coincidence event was registered between the two paddles. The timing information of each valid K600 event was used to measure the time of flight (TOF) of the protons through the K600, the drift times in the drift chambers and for the coincidence measurement between the K600 and the silicon detector telescope.

2.2.2 Silicon detector telescope

The silicon detector telescope was mounted inside the 524 mm diameter K600 scattering chamber as shown in figure 2.1. This detector telescope consisted of three silicon surface barrier detectors, which are referred to as the ΔE, E and veto detectors. The ΔE detector had a thickness of 94.8 μm and is used to measure the energy-loss of the particle as it passes through it. The second detector had a thickness of 2027 μm, which is thick enough to stop alphas up to 66.31 MeV and ^{3}He up to 61.07 MeV, respectively. Those particles that do not stop in the E detector will pass through to the veto detector, which had a thickness of 1017 μm. A schematic diagram of the detector telescope is shown in figure 2.2. The veto detector was used to discard mainly the high-energy protons to reduce the overall event rate. The choice of the thickness of the ΔE and E detectors was determined by the energy range of the quasi-free scattered alpha particles at the angles of 40.1^{0}, 45.5^{0} and 51.5^{0} as shown in table 2.1. Silicon detectors were chosen since they have energy resolutions of better than 100 keV. The low energy threshold of the alpha was 13 MeV and the high-energy threshold was

66.31 MeV. For energies greater than 66.31 MeV the alpha event are discarded by the veto detector. A collimator of 7.2mm in diameter was placed between the target and the telescope at a distance of 131.24mm from the target. The collimator defined the solid angle of detection. The solid angle is calculated from the equation

$$\Delta\Omega = \frac{\pi r^2}{x^2}$$

where r =3.6 mm is the radius of the collimator and x = 131.24 mm is the distance from the target to the back of the collimator. The size of the solid angle was found to be 2.36 msr. The angular acceptance defined by the solid angle was 3.14^0. The collimator was made of brass with a thickness of 2.1cm, which was thick enough to stop 100 MeV protons.

Figure 2.1: *Picture showing the silicon detector telescope inside the scattering chamber.*

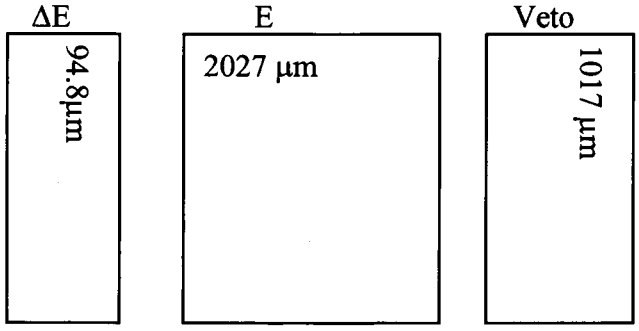

Figure 2.2: *Schematic diagram of the silicon detector telescope.*

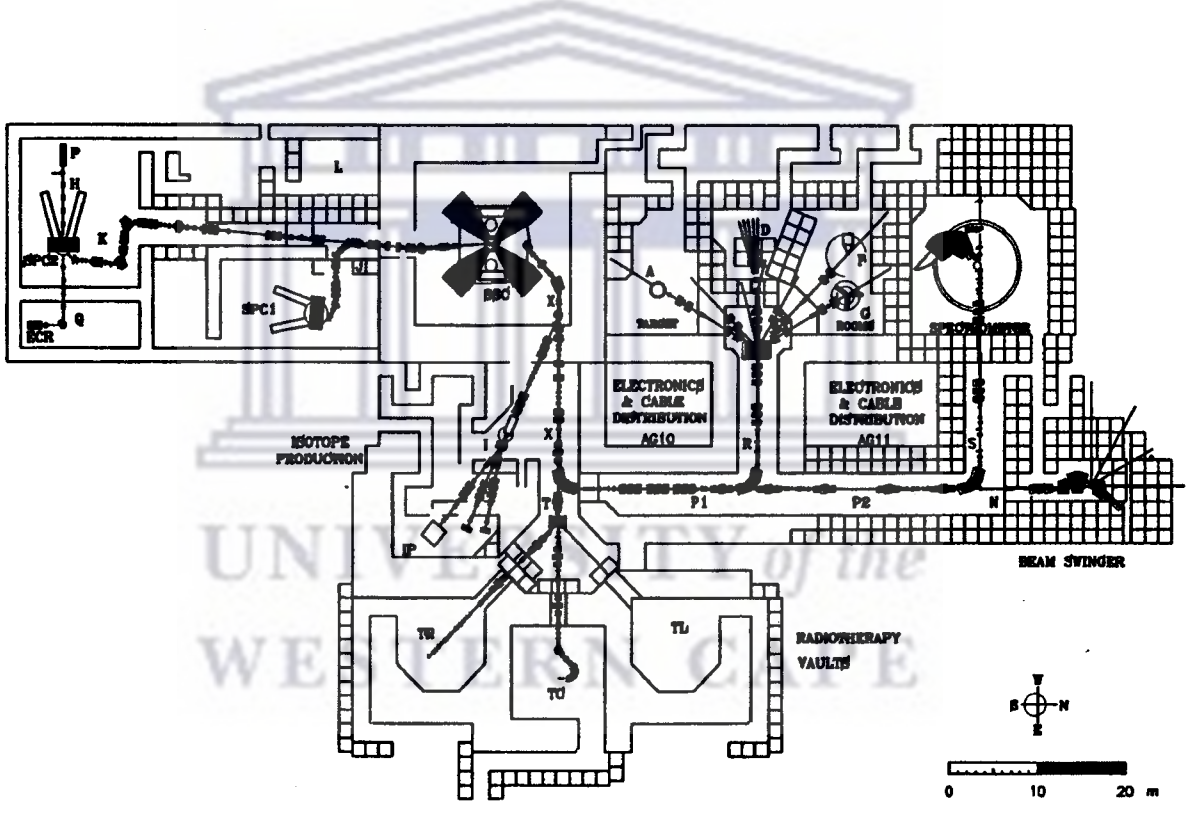

Figure 2.3: *Layout of the iThemba LABS cyclotron facility indicating the location of the spectrometer vault.*

2.3 Polarized Proton beam

The cyclotron facility of iThemba LABS is a multidisciplinary institute providing particle beams used for nuclear physics, isotope production and radiotherapy. For this experiment a beam of polarized protons from the polarized ion source (PIS) was injected into the solid-pole light-ion injector cyclotron (SPC2) and accelerated to an energy of 4.55 MeV. These protons were then injected into the Separated Sector Cyclotron (SSC) in which the protons were accelerated to an energy of 100 MeV. After extraction from the SSC the 100 MeV protons were transported first along the X beam line, where a dipole magnet bent the beam into the P1 and P2 beam lines. Quadropule and steering magnets are used along the beam lines to direct the beam. After the P2 beamline the beam was bent into the S-line and delivered onto the target inside the K600 scattering chamber.

The beam polarization was measured using elastic scattering from a target for which the value of the analyzing power (A_y) is known. To determine the beam polarization at low beam energies a ^{4}He target was used in the K-line polarimeter while at the high energies a $(CH_2)_n$ target was used in the P-line polarimeter.

The K-line polarimeter consists of a gas cell containing high purity helium gas and is equipped with an entrance and exit window of Havar. Two silicon detectors were positioned at $\theta_{lab}=110^0$ on either side of the beam direction. In the K-line the $^4He(\vec{p},p)$ elastic reaction was used for 4.307 MeV incident polarized protons. The analyzing power for this reaction is 0.93 [Sch71]. The K-line polarimeter was used to optimize the degree of polarization and to assist with the tuning of the ion source prior to the experimental runs.

The P-line polarimeter consists of a 75μm thick $(CH_2)_n$ foil mounted on a target ladder situated in a dedicated scattering chamber in the P-line. Two sodium iodide detectors were mounted at 40^0 on either side of the beam direction. Elastic scattering in the $^{12}C(\vec{p},p)$ reaction was used in the P-line in the case of 100 MeV polarized protons with an analyzing power of 0.74 [För06]. The P-line polarimeter was used to determine the beam polarization during the experiment:

$$p^{\uparrow} = \frac{\varepsilon_1}{A_y}$$

where $\varepsilon_1 = \frac{L^{\uparrow} - R^{\uparrow}}{L^{\uparrow} + R^{\uparrow}}$

and $p^{\downarrow} = \frac{\varepsilon_2}{A_y}$

where $\varepsilon_2 = \frac{L^{\downarrow} - R^{\downarrow}}{L^{\downarrow} + R^{\downarrow}}$

where $A_y \equiv$ known analyzing power

$p^{\downarrow} \equiv$ Spin-down.

$p^{\uparrow} \equiv$ Spin-up.

$L^{\uparrow\downarrow}$ ≡ the number of elastic scattered events registered in the left detector associated with the incoming particles with upward and downward beam polarization, respectively.

$R^{\uparrow\downarrow} \equiv$ the number of elastic scattered events registered in the right detector associated with the incoming particles with upward and downward beam polarization respectively.

The beam polarization values for spin-up, spin-down and their averages are summarized in Table 2.2.

Table 2.2: *Values of the spin-down ($p^{\downarrow}$), spin-up ($p^{\uparrow}$) beam and average beam polarization.*

	$p^{\downarrow}$ [%]	$p^{\uparrow}$ [%]	Average polarization [%]
Weekend 1	49.85	71.58	60.71
Weekend 2	87.70	74.20	80.95
Weekend 3	83.50	78.45	80.98
Weekend 4	82.00	71.90	76.95
Weekend 5	83.90	77.10	80.5

2.4 Scattering Chamber

The scattering chamber of 524 mm in diameter is mounted at the turning axis of the spectrometer. The targets were mounted at the center of the scattering chamber on a target ladder that can hold six different targets. Any one of these targets can be positioned in the beam by changing the position vertically. The target ladder can also be rotated to a different direction with respect to the beam.

The scattering chamber has various ports, which are used for different purposes of which two connect the incoming beamline and the 10m long beam pipe to the beam stop. Another perspex-covered port allows a closed circuit television camera to view the scintillating target assisting the operators while focusing the beam in the control room. Another port provides cable feed-throughs, which were used to connect cables from the silicon detectors to the preamplifiers, which were mounted directly to the feed-throughs outside the scattering chamber.

2.5 Targets

^{40}Ca targets of different thickness of 2.65 mg cm^{-2} ,2.38 mg cm^{-2} and 3.87mg cm^{-2} ,respectively, were mounted on aluminium frames each with an opening of 25mm in diameter. The ruby target with a hole of 3mm in diameter was used to align the beam and focus the beam spot of less than 3mm in diameter through a hole at the center of the target. A $(CH_2)_n$ target was used for tuning the electronics by providing an enhanced number of coincidence events between the incident proton and the recoiling proton in elastic p-p scattering. An empty target was used for beam halo monitoring. The halo which was tolerated from an empty target was not more than 30 counts per second at a beam intensity of about 30 nA.

2.5.1 Target thickness measurements

A ^{228}Th source was placed in front of the target while a silicon detector measured the transmitted alpha particles behind the target. The measuring system was first calibrated without a target recording detector channel numbers of the corresponding alpha energies. The 8.78 MeV energy peak was used. The same procedure was repeated with a ^{40}Ca target in position. The thickness of the ^{40}Ca targets were determined by measuring the energy loss of the alpha particles from a ^{228}Th source in the targets. The conversion from the corresponding range of the alphas in ^{40}Ca to the thickness was performed with the ELOSS program [Jip84]. The list of the channel number, energy loss and the thickness of ^{40}Ca targets are shown in Table 2.3.

Table 2.3: *The channel number corresponding to the 8.78 MeV energy peak, energy loss and the thickness of ^{40}Ca targets.*

Target	Position (ch#)	Eloss (MeV)	Thickness (mg cm^{-2})
Empty	660.0	0.00	
A (^{40}Ca)	571.0	1.113	2.65
B (^{40}Ca)	529.3	1.667	3.87
C (^{40}Ca)	580.6	0.99	2.38

2.6 Electronics

The electronic set-up which was used to process the signals of the alpha and ^{3}He pre-scaled singles events as well as pulser events will be discussed in the following subsections.

2.6.1 Detector signals and pre-amplifiers

The signals of all three Si detectors were processed by charge sensitive preamplifiers (PREAMP) to produce timing and linear signals. These preamplifiers are usually

mounted as close as possible to the detector in order to minimize noise pickup. In this experiment the preamplifiers were mounted to the feed-throughs outside the scattering chamber.

2.6.2 Linear signals

The linear signal from the preamplifier (AMP) gives information on the energy of the particle detected. Every linear signal was processed by the amplifier as part of the electronic set-up in the data room. The amplifier amplified and shaped the linear signal before passing it to the delay amplifier followed by the linear gate and stretcher (LGS) module. Only for a valid event as defined by the corresponding timing signals a logical gate allowed the linear signal to pass the LGS to be digitized by the analog-to-digital converter (ADC) module as illustrated in figure 2.4.

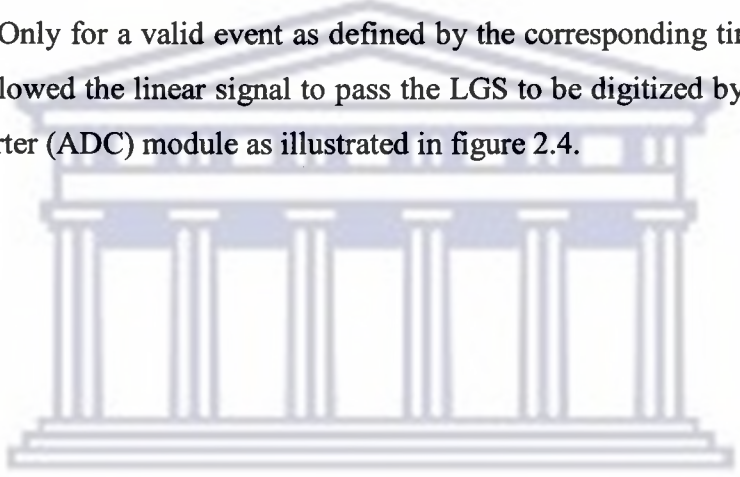

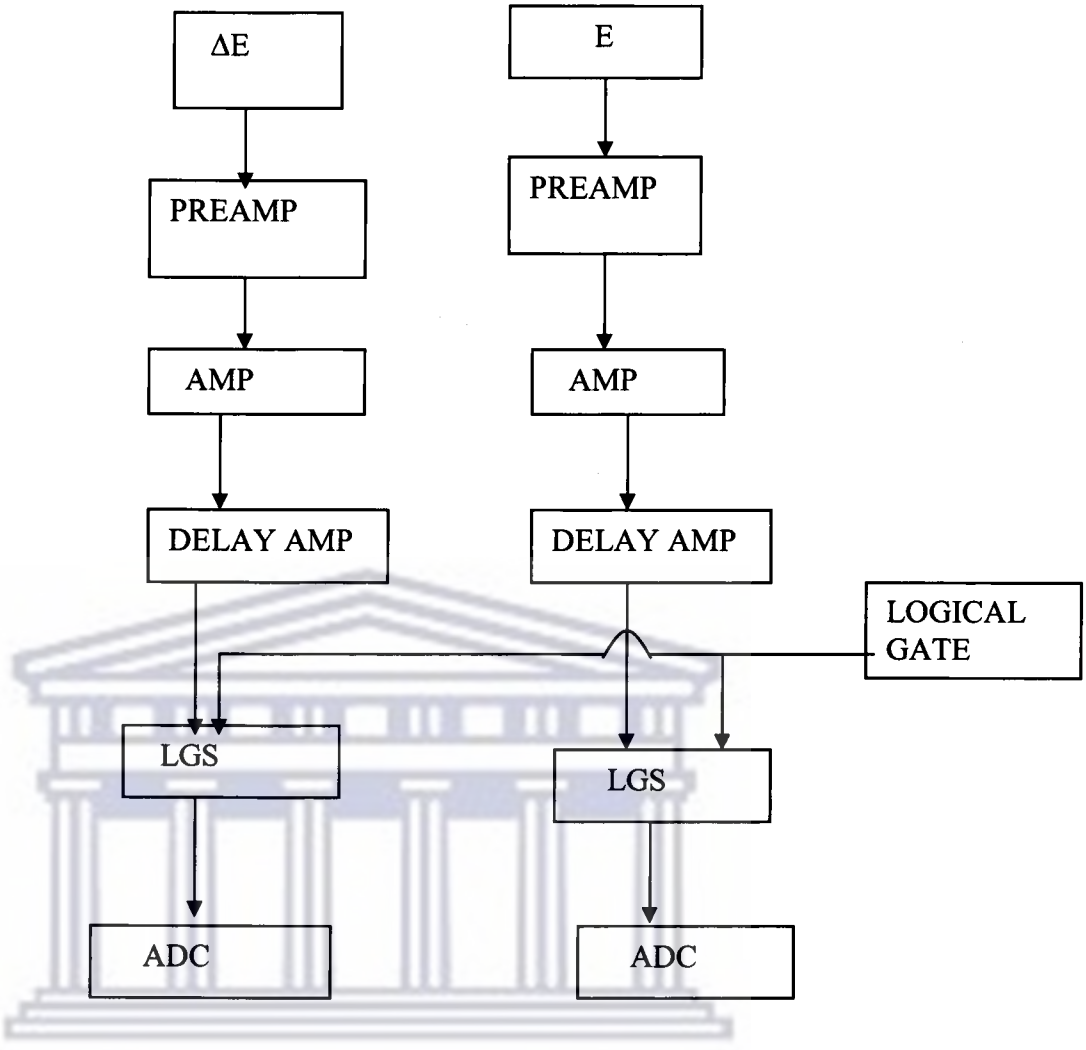

Figure 2.4*: Electronic diagram for processing the linear signals from the ΔE and E detectors.*

Table 2.4*: Table showing the electronic modules used for processing the linear signals.*

Module	Model
Preamplifier (E-detector)	ORTEC 142A
Preamplifier (ΔE-detector)	ORTEC 142B
Amplifier	ORTEC 572
Delay Amplifier	ORTEC 427A
Linear Gate and Stretcher	ORTEC 442
Analog-to-digital converter	CANBERRA 8077

2.6.3 Timing signals

Each timing signal from the preamplifier was processed by a timing filter amplifier (TFA) followed by a constant fraction discriminator (CFD) to convert it to a logic signal. The logic signal from each detector was used to determine whether an event is valid or not. The valid events were coincidence events, pre-scaled singles telescope events, pre-scaled K600 events and pulser events. The logic signals of the ΔE and E detectors must be in coincidence with each other and in anticoincidence with the veto detector ($\Delta E \cap E \cap \overline{V}$) in order to register a valid telescope event. For an event to be discarded the veto detector is in coincidence with the ΔE and E detector ($\Delta E \cap E \cap V$). The veto detector was used to reduce the event rate by discarding mainly the high-energy protons. These operations were obtained with a 4-fold logic unit. The output signals from the 4-fold logic unit were fed to a prescaler. Pre-scaled singles events represented 5% of all the events in the silicon detectors. The logic signal for a valid event was passed on to the gate and delay generator (GDG) to generate a gate for processing the linear signals as well as to the event trigger as illustrated in figure 2.5. The logic signal for a valid telescope event was used to process telescope pre-scaled singles and pulser events and to establish whether there is a coincidence between the telescope and K600.

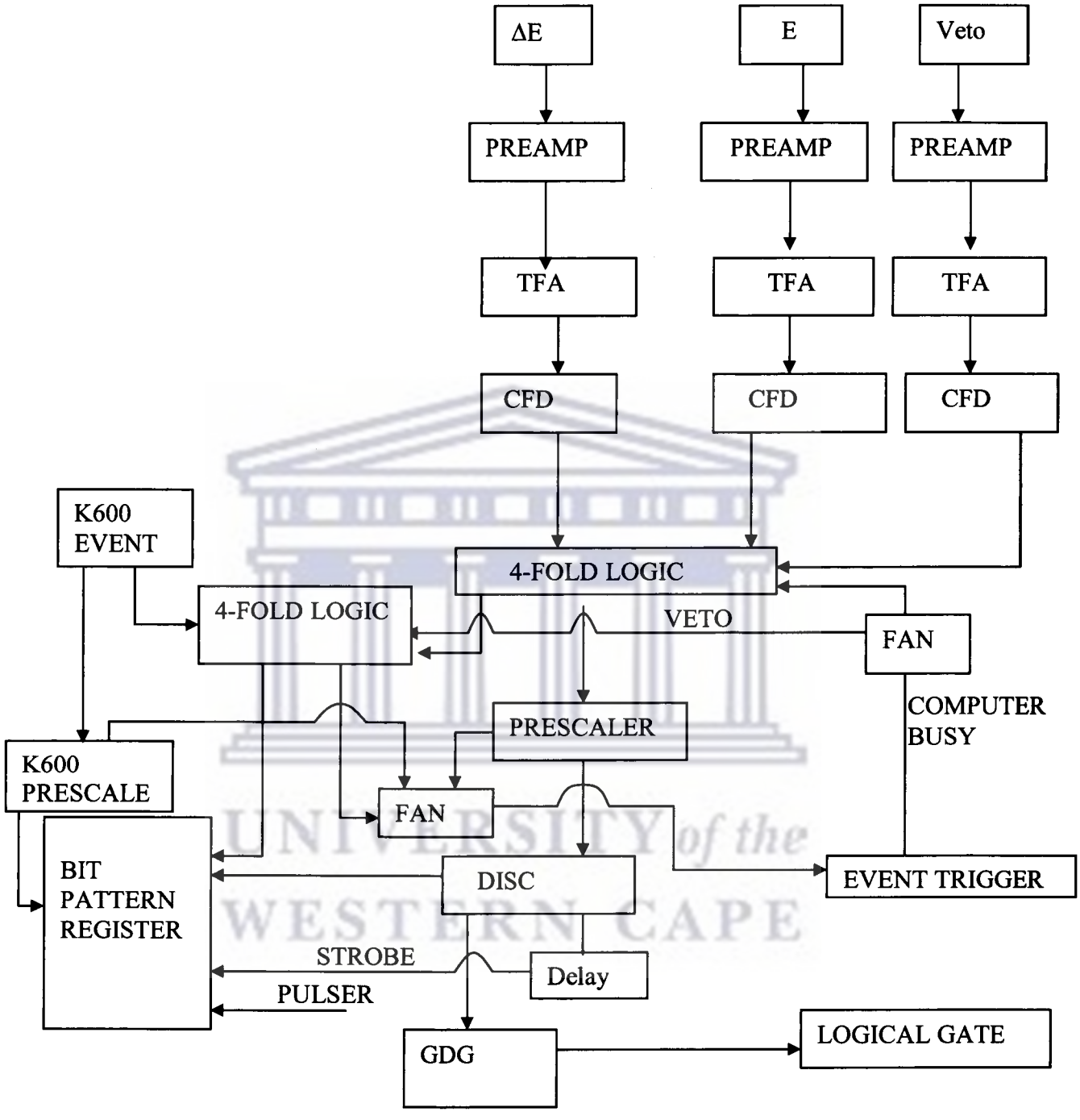

Figure 2.5: *Electronic diagram for the timing signals from ΔE, E and veto detectors for processing the pre-scaled singles events.*

Table 2. 5: *Table showing the electronic modules used for processing the timing signals.*

Module	Model
Preamplifier (ΔE)	ORTEC 142B
Preamplifier (E, Veto)	ORTEC 142A
Timing Filter Amplifier (TFA)	ORTEC 474
Constant Fraction Discriminator	ORTEC 436
Timing Single Channel Analyzer (TSCA)	ORTEC 551
4-Fold Logic Unit (4-FLU)	LECROY 365AL
Gate and Delay Generator (GDG)	ORTEC 416A
Discriminator	LECROY 821
Timer	ORTEC 719

2.7 Current integrator

The proton beam current measured by the beam stop was fed to a Brookhaven Instrument current integrator (BIN 1000C) module. This electronic module gives an output that is proportional to the beam current. It allows selection of the current integrator range which determines the number of pulses output for each unit of accumulated charge measured and enables the position of the selected range to be read by the computer via a CAMAC interface during data acquisition. The current integrator determines the total charge of the proton beam accumulated in the beam stop. The total accumulated charge of the proton beam was used to calculate the double differential cross sections.

2.8 Pulser

The pulser signal was generated from the digital output of the current integrator. A prescaled current integrator signal triggered a tail pulse generator of which the output was sent to the test input of the detector preamplifiers. The pulser rate was therefore proportional to the beam current. The aim of the pulser is to determine the electronic dead time. The ratio of the inhibited pulser scaler and the pulser peak counts actually observed in a pulser spectrum gives the electronic dead time.

2.9 Event Trigger

Events of interest were accepted in an event trigger unit module, which enters the computer via a CAMAC module. These events were identified in the bit pattern register as coincidence, pre-scaled singles and pulser events. The event trigger enters the computer and initiates the event read–out cycle, which is carried out by the data acquisition program.

2.10 Computer busy

The computer busy signal was generated by the event trigger module for every valid event. The computer busy signal inhibits one set of the scalers, which prevents these scalers from updating while read-out cycle is in progress. The computer busy signal was also fanned out in order to veto the logic part of the circuit.

2.11 Scalers

The scalers are read out by the computer via a CAMAC module. Two sets of scalers were used which represented the inhibited and uninhibited scalers. The uninhibited scalers counted the total number of events detected in the telescope, total accumulated

charge, pulser events and the output from the current integrator. In a separated module these scalers were inhibited by the computer busy signal.

2.12 Bit Pattern register

Valid events were identified in the bit pattern unit as coincidence, prescaled singles telescope, prescaled singles K600 and pulser events by associating every accepted event with a certain bit. The bit pattern unit was read out upon arrival of a strobe signal. The strobe signal is a version of the delayed event trigger signal. The information from the bit pattern register is needed to structure the order in which a data word was built up.

2.13 Clock

A continuously running timer was used to monitor the computer dead time. The computer dead time was calculated by dividing the inhibited scaler value by the unhibited scaler value of the clock.

CHAPTER 3 DATA ANALYSIS

3.1 Introduction

For every valid prescaled singles telescope event, the ΔE-E particle identification technique was applied in order to determine the charged particles such as protons, deuterons, tritons, ^{3}He and alpha emitted in the reactions induced by 100 MeV protons on ^{40}Ca. The aim of the analysis of the experimental data was to extract the double differential cross sections of the ^{3}He and ^{4}He particles from the prescaled singles data set. In this chapter the experimental analysis of the emitted ^{3}He and alpha particles is described.

3.2 Data acquisition program

The XSYS [Yod94, Pil96] software package was used for event-by-event data replay and data acquisition. XSYS operates on a VAX computer system. The data acquisition and replay is controlled by the sorting subprocess which reads an EVAL and COM file. The EVAL file provides a language used for sorting data either online or from event-by-event data files. The different steps, which were taken before acquiring data, were as follows. After running XSYS, the VME files were loaded followed by loading the COM file and EVAL file. The VME system is used to link the information between the different CAMAC modules like the ADC's, Bit pattern register, event trigger and scaler modules with the computer system for data acquisition. The COM file defines the data areas for various histograms to be stored and defines the data areas for 1-dimensional and 2-dimensional gates. The EVAL program sorted and analysed pre-scaled singles events amongst other, the data of the charged particles that were measured in the ΔE and E detectors.

3.2.1 Online Data Taking

Once the 100 MeV proton beam was delivered to the K600 scattering chamber, the first step of online data taking was to align the beam spot to the centre of the target by using the ruby target as described in section 2.5. After the beam spot was properly aligned on the target, the beam halo was monitored using an empty target. The beam was accepted if the count rate ratio from the empty target and ^{40}Ca target was less than 5 %. The *H (p, p) H* reaction was used for the tuning of coincidences between the telescope and K600. The K600 was placed at an angle of 29^0 while the telescope was placed at an angle of 59^0 determined by the kinematics for elastic proton scattering off hydrogen. Tuning of coincidences between the telescope and K600 was set up by measuring the scattered proton in the K600 and the recoiling hydrogen nucleus in the silicon detector telescope in order to get the coincidence timing.

The energy calibrated of the K600 was carried out by means of elastic and inelastic scattering of 101.3MeV protons on ^{12}C. Data were collected in two-hour runs over four weekends. After every run the polarization of the proton beam was measured in the high-energy beamline using the P-line polarimeter (see section 2.3). The different thickness of ^{40}Ca targets and quasi-free angles for the different weekends are shown in table 3.1.

Table 3.1: *Summary of quasifree angles and thickness of ^{40}Ca targets used during the experiment.*

Quasifree angles		Weekend	^{40}Ca target (mg/cm^2)
K600 angle	Telescope angle		
59^0	-51.5^0	2	2.38
59^0	-51.5^0	3	2.38
70^0	-45.45^0	3	2.38
70^0	-45.45^0	4	2.65
81^0	-40.12^0	4	2.65
81^0	-40.12^0	5	3.87

3.2.2 Data replay

The software which was used for data acquisition was also used for the event-by-event data replay. The COM and EVAL files were extended by defining additional data areas for the particle identification gates, mass function gates and energy spectra.

3.3 Energy Calibrations

A ^{228}Th source was used for the energy calibrations of the silicon detectors. As an example the alpha energy spectrum which was measured with the ΔE Si detector is shown in figure 3.1. By using XSYS the channel number for each energy peak was determined. The channel numbers were plotted versus energies. The calibration formulas for the ΔE and E detector were obtained from linear fits to these graphs using the PHYSICA programme [Chu94]. The calibration formula of the ΔE detector is

$$E = (1.33031956 \times 10^{-2}) \text{ ch \#} + 8.12839607 * 10^{-2} \quad (3.1)$$

while for the E detector it is

$$E = (1.54279846 \times 10^{-2}) \text{ ch \#} - 7.04632451 * 10^{-2} \quad (3.2)$$

where ch# corresponds to the channel number.

The calibration curve for the ΔE detector is shown figure 3.2. The calibration parameters for the slope and offset of the ΔE and E detector are summarized in table 3.2.

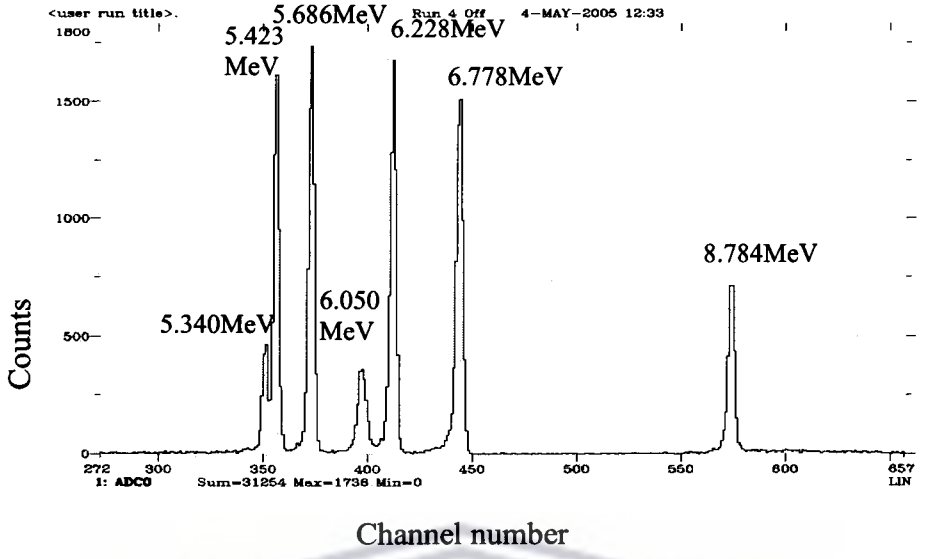

Figure 3.1*: Energy spectrum of the alpha particles from a ^{228}Th source as measured with the 94.8μm silicon ΔE detector. The indicated energies are in MeV.*

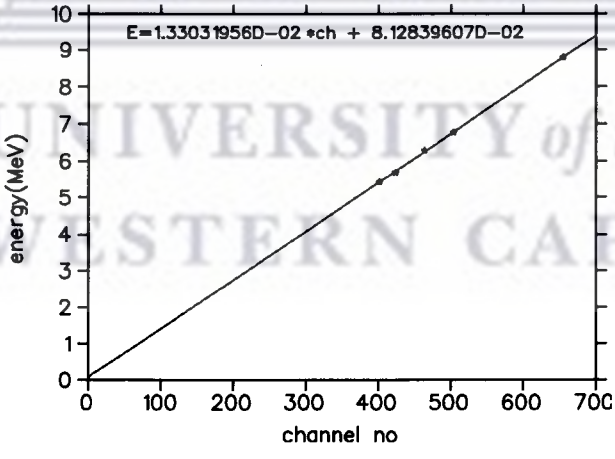

Figure 3.2*: Energy calibration fit (solid line) of the alpha particle energies (symbols) in ΔE detector. Also shown are the corresponding calibration parameters for the slope and offset.*

Table 3. 2: *Calibration parameters of the ΔE and E detectors.*

Detector	Slope	Offset
ΔE	0.01330	-0.08128
E	0.01542	-0.07046

3.4 Particle Identification (PID)

The first step during data acquisition as well as data replay was the identification of the charged particles detected by the silicon telescope. The charged particles such as ^{3}He and ^{4}He were identified by using the ΔE-E technique. This method is used for charged particle identification and makes use of at least two detectors, normally referred to as the ΔE and E detector. The ΔE detector is used to measure the energy-loss of the particle and the charge as it passes through and the E detector measures the energy of the stopped particle. Alpha particles lose more energy than protons because alphas have a higher atomic number than protons. According to the Bethe-Bloch formula [LEO87] the energy-loss of a particle in the detector medium increases with the atomic number with decreasing energy as well as increasing mass. The ΔE detector and E detector must be coincidence in order to register a valid event. The low energy threshold depends on the thickness of the ΔE detector. In this experiment the thickness of the ΔE detector was 94 μm, which corresponds to energy thresholds of 13 MeV for alpha and 11 MeV for ^{3}He particles, respectively.

A two-dimensional particle identification spectrum (PID) was constructed by plotting the pulse height of the ΔE detector against the pulse height of the E detector. The PID spectrum was constructed from the one-dimensional spectrum of the ΔE detector and E detector. The one-dimensional spectrum of the ΔE detector had 1024 channels, which were reduced by a factor of 4 to give 256 channels, while the one-dimensional spectrum of the E detector had 8192 channels, which was reduced by a factor of 32 to also give 256 channels. Loci corresponding to the different charged particles such as protons, deuterons, tritons, ^{3}He, alpha and ^{6}He particles are recognizable in the

particle identification (PID) spectrum as can be seen in figure 3.3. The PID with a gate around the Z=2 particles is also shown in figure 3.3. Because the loci for the alpha and ^{3}He particles are close to each other a mass function was defined in order to have a better separation between the alpha and ^{3}He particles (See fig 3.4). The mass function is defined as

$$MF = [(E_A+E_B)^{1.7}-(E_B)^{1.7}] \times M_s-M_c \quad (3.3)$$

where

E_A=energy deposited in ΔE detector

E_B=energy deposited in E detector

K=constant, its value was found to be 1.7

M_s and M_c=slope and offset parameters

The values of M_s and M_c were chosen for the best separation between the ^{3}He and ^{4}He particles. The energy spectra of ^{3}He and alpha particles were obtained by setting a gate around each of the two loci in the mass function spectrum as shown in figure 3.4. The total energy of the charged particles was obtained by using the calibration equations for both detectors and by summing the energy from the ΔE and E detector. Total energy spectra of the ^{3}He and ^{4}He particles are shown in figures 3.5 and 3.6, respectively.

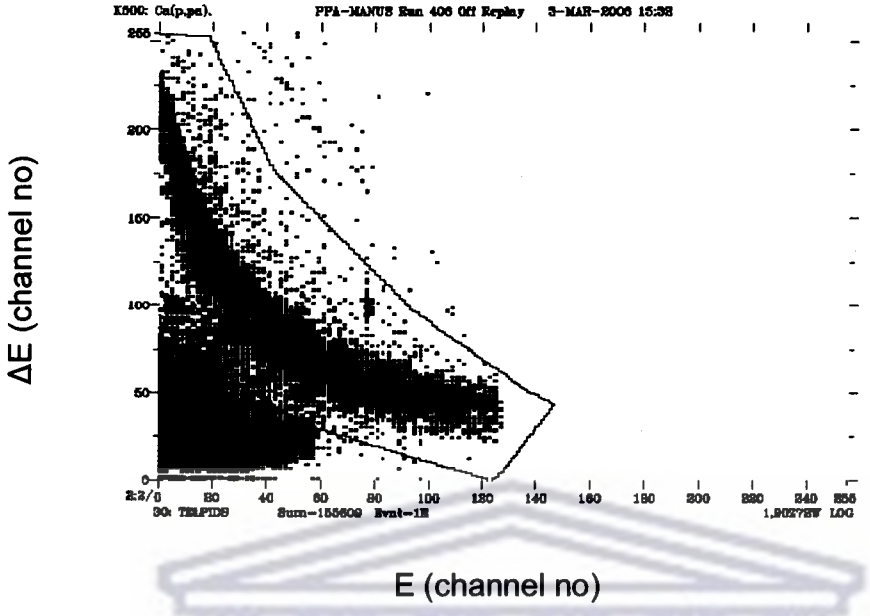

Figure 3.3: *Particle identification spectrum of ΔE versus E with a gate around the Z=2 locus.*

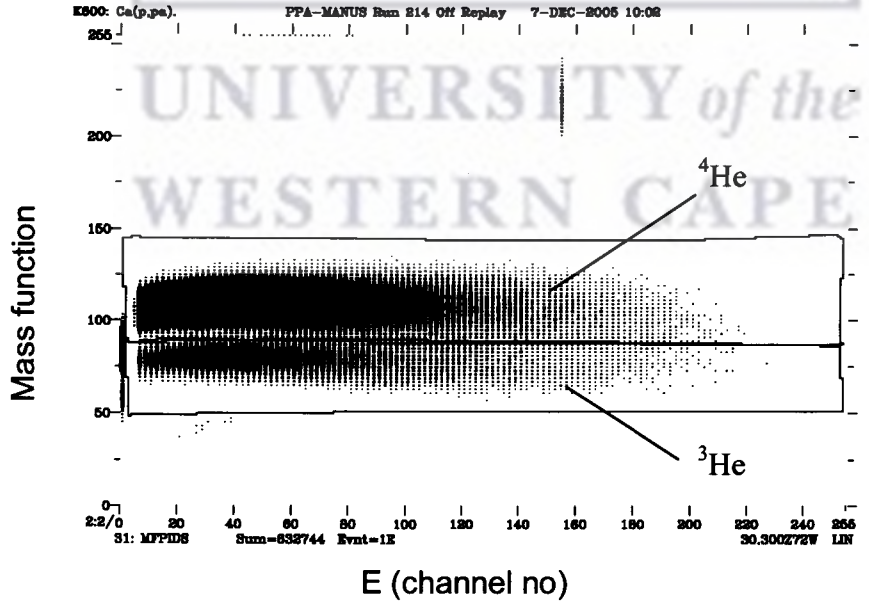

Figure 3.4: *Mass function spectrum showing gates set around the ^{3}He and ^{4}He loci.*

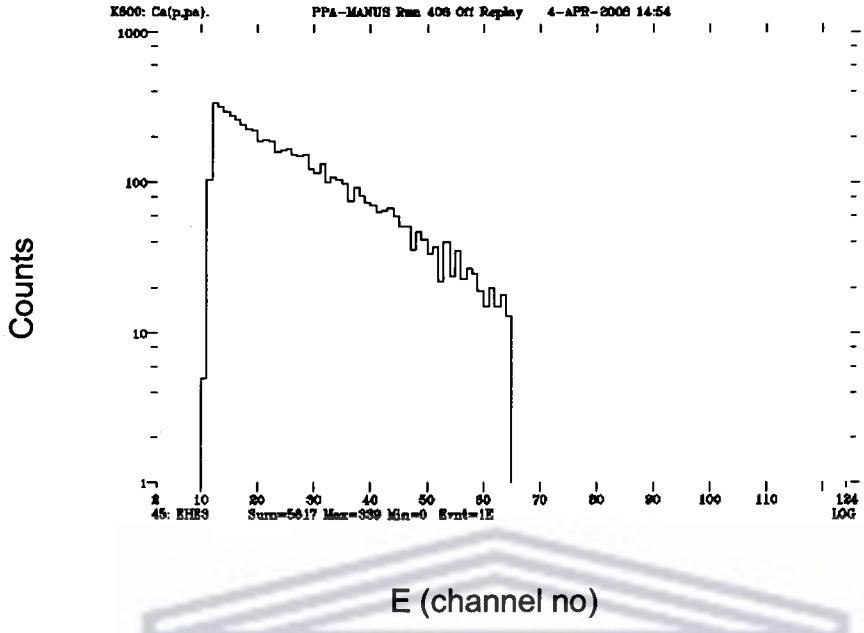

Figure 3.5*: Raw energy spectrum of ^{3}He indicating the low and high-energy threshold.*

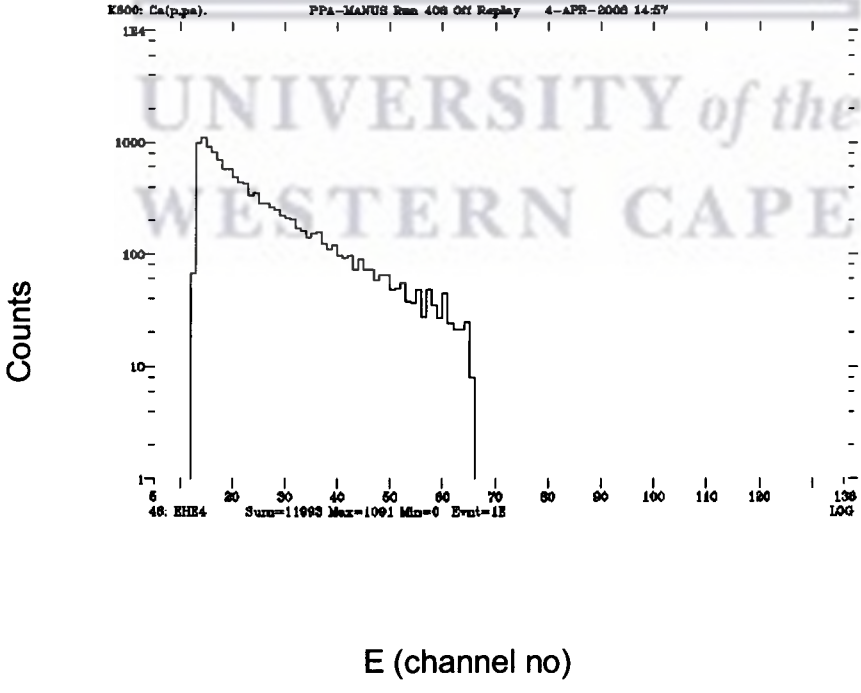

Figure 3.6: *Raw energy spectrum of ^{4}He indicating the low and high-energy threshold.*

3.5 Error analysis

3.5.1 Statistical error

The statistical error is related to the uncertainty in the counting rate. The statistical error is given by $\sqrt{N}$ where N is the number of counts in each bin. The error bars in the double differential cross sections represent the statistical errors.

3.5.2 Systematic errors

The systematic errors in the double differential cross section spectra were estimated from the uncertainty in electronic dead time, target thickness, solid angle, energy calibration, particle identification and current integrator.

Electronic dead time

The uncertainty in the electronic dead time was estimated to be 1%.

Solid angle

The uncertainty in the solid angle is due to the uncertainty in the radius of the collimator and the distance from the target to the back of the collimator. Its value was estimated to be 5 %.

Target thickness

The uncertainty in the thickness of the ^{40}Ca targets was estimated to be 1%.

Current integrator

The uncertainty of the amount of charge collected by the current integrator was found to be less than 0.2%.

Calibrations

The uncertainty in the energy calibration resulted from the slope and offset values obtained with a linear fit. The uncertainty was estimated to be 1%.

Particle identification

The uncertainty in the particle identification was obtained by setting different gates around a specific locus in the particle identification spectrum. This uncertainty was estimated to be 1.3%.

The total systematic error is the square root of the sum of the quadratures.

Table 3.3: Summary of the systematic errors.

Cause of systematic error	Error in %
Solid angle	5.0
Target thickness	1.0
Current integrator	0.2
Energy Calibration	1.0
Electronic dead time	1.0
Particle identification (PID)	1.3
Total systematic error	5.5

3.6 Conversion to absolute cross sections

The inclusive double differential cross section spectra of the ^{3}He and ^{4}He particles were obtained by using the equation

$$\frac{d^2\sigma}{d\Omega dE} = N_c.P.K \quad \text{in } [\mu b\ sr^{-1}\ MeV^{-1}] \tag{3.4}$$

where

$N_c \equiv$ the number of counts in each energy bin

$P \equiv$ normalization of 5% of the prescaled singles events

$K \equiv$ the normalization factor calculated from

$$K = \frac{1}{\Delta\Omega.\Delta E.d_t.N_0.\rho}$$

where

$\rho \equiv$ number of ^{40}Ca nuclei per unit area of target thickness in μb

$N_0 \equiv$ number of protons in beam

$\Delta\Omega \equiv$ solid angle in sr

$\Delta E \equiv$ bin size in MeV

$d_t \equiv$ electronic dead time

while N_0 and ρ are defined as follows

$$N_0 = \frac{C}{e}$$

where

$C \equiv$ the total charge of the proton beam accumulated in the beam stop

$e \equiv$ the charge of the proton.

$$\rho = \frac{M(g)N_A}{M}$$

where

$M(g) \equiv$ the thickness of ^{40}Ca in mg/cm^2

$N_A \equiv$ Avogadro's number (6.022×10^{23})

$M \equiv$ the atomic mass number of ^{40}Ca.

The double differential cross sections (μb sr^{-1} MeV^{-1}) were calculated by converting the number of counts in each energy bin of the energy spectra of ^{3}He and ^{4}He according to equation 3.4. The conversion to double differential cross sections calculations were done separately for each scattering angle since each angle has different values of total charge of the proton beam accumulated in the beam stop and statistical error. In the case where average cross sections were obtained of cross sections from different weekends or different target thickness (see Figs 3.7 and 3.8) the weighted mean method was used [Leo87]. The average cross section N was calculated as follows:

$$N = \frac{N_a/\sigma_1^2 + N_b/\sigma_2^2}{1/\sigma_1^2 + 1/\sigma_2^2} \qquad (3.5)$$

where

N_a and N_b are the cross sections which were obtained from two different measurements. σ_1 and σ_2 are the statistical errors obtained from these two measurements.

The average statistical error was calculated from

$$\sigma^2 = \frac{1}{\frac{1}{\sigma_1^2} + \frac{1}{\sigma_2^2}} \qquad (3.6)$$

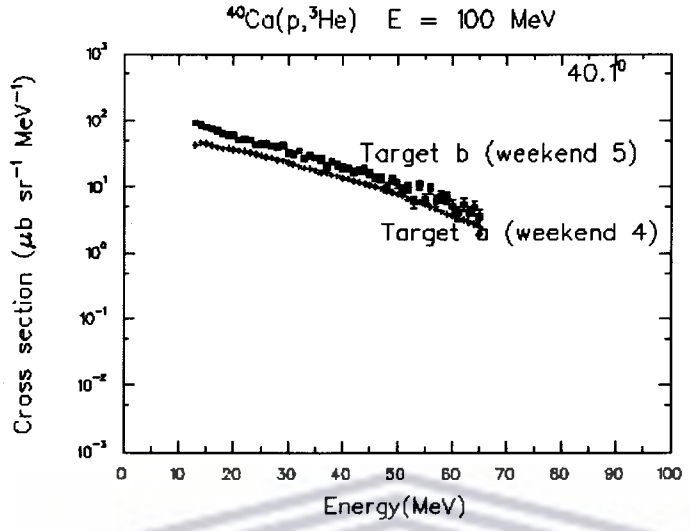

Figure 3.7*: Double differential cross sections of ^{3}He emitted from the reaction of 100 MeV protons on ^{40}Ca with different thickness at an emission angle of 40.1^{0}. Target a had a thickness of 2.65 mg cm^{-2} while target b had a thickness of 3.87mg cm^{-2}.*

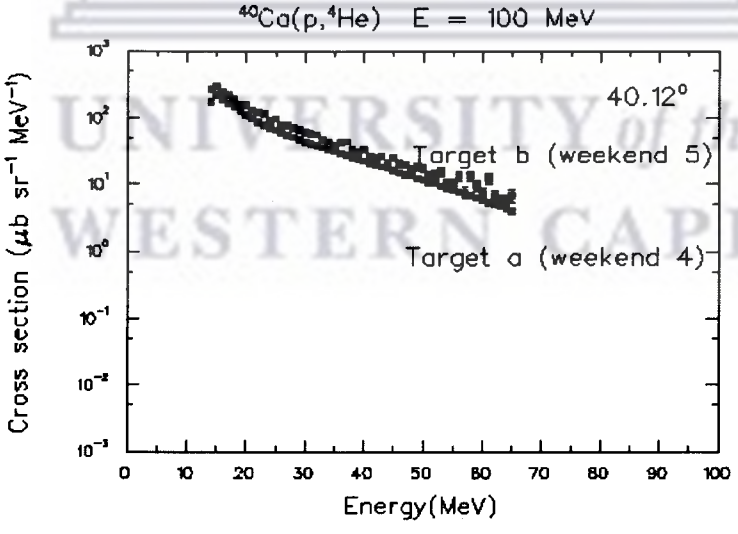

Figure 3.8*: Double differential cross sections of ^{4}He emitted from the reaction of 100 MeV protons on ^{40}Ca with different thickness at an emission angle of 40.1^{0}. Target a had a thickness of 2.65 mg cm^{-2} while target b had a thickness of 3.87mg cm^{-2}.*

CHAPTER 4 Calculations

The experimental double differential cross section spectra of the emitted alpha and ^{3}He particles at emission angles of 40.1^{0}, 45.5^{0} and 51.5^{0} were compared to both the phenomenological prescription of Kalbach as well as the exciton model preequilibrium code PRECO-2000. Details of these theoretical calculations will be described in this chapter.

4.1 Kalbach Systematics

The Kalbach-Mann (K-M) systematics were initially developed to describe the shape of the angular distributions of inclusive reactions at incident energies up to 80 MeV and emission energies up to 60 MeV [Kal88]. The angular dependence of the inclusive reactions was established, at least to first order, to be independent of the bombarding energy as well as the nature of the projectile, target and the emitted particle. The Kalbach-Mann (K-M) systematics were parameterized in terms of Legendre polynomials using a small number of universal parameters. The shape of the angular distribution is determined by the energy of the emitted particle and the fraction of the time that it was emitted in a multistep direct (MSD) process rather than the multistep compound (MSC) one. All the polynomials contribute MSD component while only even order polynomials are used for the MSC process. In these parameterizations of pre-equilibrium cross sections Kalbach-Mann distinguish between the MSC and the MSD reactions [Kal81].

The high-energy limit of the K-M systematics occurs at emission energies of around 50 MeV. As the emission energy increases the experimental cross sections decrease by up to a factor of one hundred over the angular range of the emitted particle.
Hence the smooth curve which has to describe the yield at the backward angles can no longer be fixed by a set of Legendre polynomials. At incident energies larger than 90 MeV an infinite number of polynomials were needed in the systematics [Kal88].

For nucleon and alpha particle induced reactions on targets that range from ^{12}C to ^{232}Th at incident energies up to 720 MeV leading to emitted particles with mass numbers up to four, improvements and extension of the Kalbach –Mann (KM) systematics were performed by Kalbach and are summarized in [Kal88]. The Kalbach-Mann (K-M) systematics were changed by replacing the Legendre polynomials with an expression of exponential decay as a function of the emission angle θ. An exponential in cosθ was chosen because it describes the smooth yield of the cross section at 0^0 and 180^0, while the solid angle is expressed as $d\Omega = d\cos\theta d\phi$. The mathematical form of the multistep direct (MSD) and multistep compound (MSC) part of the angular distributions requires that the angle integration yields the correct energy differential cross sections.

Since for incident energies higher than 100 MeV quasifree scattering becomes increasingly important, the experimental data with features from quasifree scattering have been omitted from the parameterization.

For incident proton energies up to around 100 MeV and for incident alpha particle energies up to 160 MeV the angular distributions are determined by the emission energy, target mass, bombarding energy and type of the emitted particle [Kal88]. For incident proton energies between 100 and 165 MeV there is a change in the physical parameter determining the shape of the angular distributions. The ratio $\frac{e_b}{e_a}$ of the energy in the exit (e_b) to the energy in the entrance (e_a) channel was found to show good improvement in the parameterization for proton energies above 100 MeV. As emission occurs from the excited nucleus the effects of pairing and shell structure which have influences on the position of the ground state Fermi level is less important. The parameter e_b is replaced by

$$e_b' = \epsilon_b + S_b \qquad (4.1)$$

where

$S_b \equiv$ is the separation energy.

The calculations of the separation energy S_b are obtained from the liquid drop model with the pairing and shell terms neglected. The separation energy for the nucleus C into a particle b and nucleus B was calculated using the mass formulae of Myers and Swiatecki for spherical nuclei. The equation used to calculate the separation energy is given by [Kal88]:

$$S_b = 15.68(A_C - A_B) - 28.07\left[\frac{(N_C - Z_C)^2}{A_C} - \frac{(N_B - Z_B)^2}{A_B}\right] - 18.56(A_C^{2/3} - A_B^{2/3}) + 33.22$$
$$\left[\frac{(N_C - Z_C)^2}{A_C^{4/3}} - \frac{(N_C - Z_C)^2}{A_B^{4/3}}\right] - 0.717\left[\frac{Z_C^2}{A_C^{1/3}} - \frac{Z_B^2}{A_B^{1/3}}\right] + 1.211\left[\frac{Z_C^2}{A_C} - \frac{Z_B^2}{A_B}\right] - I_b \quad (4.2)$$

where

C ≡ composite nucleus

B ≡ residual nucleus

N, Z and A ≡ neutron, proton and mass number of the nuclei, respectively

I_b ≡ the energy required to break the alpha and ^{3}He emitted particles up into their constituent nucleons.

For the inclusive reaction a + A→ C→B + b where a is the incident proton, A is the ^{40}Ca target nucleus, C is the composite nucleus ^{41}Sc, B is the residual nucleus ^{37}K when the emitted particle b is an alpha and ^{38}K when the emitted particle b is ^{3}He, respectively. Values of the parameters used in eq.4.2 are listed in Table 4.1.

Table 4. 1*: List of the values used to calculate the separation energies.*

	N_C	Z_C	A_C	N_B	Z_B	A_B	S_b (MeV)	I_b (MeV)
^{40}Ca(p, α)	20	21	41	18	19	37	14.776	20.577
^{40}Ca(p, ^{3}He)	20	21	41	19	19	38	15.528	6.976

Because of the second order dependences seen with incident protons and because of the change in the slope parameter at incident energies above 100 MeV, the process of parametrizing the general shapes of the angular distribution was written as [Kal88]:

$$a(e_b') = 0.040e_b' + 1.8\times10^{-6}(e_b')^3 \ . \tag{4.3}$$

This expression was modified for the second order dependence on bombarding energy and emitted particle for nucleon induced reactions. The incident energy dependence was accounted for by adding a third term, which varies as $\left(\frac{e_b'}{e_a'}\right)^n$. Best fits including this term to existing data produced a value of 4 for the exponential. The slope parameter for both the projectile and emitted particle dependence is given by [Kal88]:

$$a(e_b') = 0.040e_b' + 1.8\times10^{-6}(e_b')^3 + 1.9M_a m_b\left(\frac{e_b'}{e_a'}\right)^4 \tag{4.4}$$

where

M_α=0

$M_n = M_p$=1

$M_n = \frac{1}{2}$

$m_p = m_d = m_t = m_{He\text{-}3}$ =1

m_α = 2

The parameter e_b' in the first two terms of equation 4.4 is replaced by the ratio $\left(\frac{e_b'}{e_a'}\right)$ so that

$$X_1 = \left(E_1\frac{e_b'}{e_a'}\right) \tag{4.5}$$

where

$$E_1 = \min(e_a', E_{t1}) \ . \tag{4.6}$$

E_{t1} is the energy at which the transition is made from an e_b' to an $\frac{e_b'}{e_a'}$ dependence. Above the emission energy of 130 MeV E_{t1} is dependent on e_b' while below 130 MeV it is dependent on $\frac{e_b'}{e_a'}$. The third term in equation 4.4 is expressed with a similar transition as the first two terms but with a lower value of E_{t3} since the angular distribution slope can vary by large amounts in a very small interval of emission energies. The slope parameter of the angular distribution in the third term in equation 4.4 depends on the emission energy and is dependent on the incident energy. The formula for the slope parameter is then given by [Kal88]:

$$a(e_b', e_a') = 0.040X_1 + 1.8\times10^{-6}(X_1)^3 + 6.7\times10^{-7}M_a m_b (X_3)^4 \tag{4.7}$$

where X_3 is defined as

$$X_3 = \left(E_3 \frac{e_b'}{e_a'}\right)$$

and

$$E_3 = \min(e_a', E_{t3}) \tag{4.8}$$

The multistep direct (MSD) part of the cross section is given by [Kal88]

$$\frac{d^2\sigma_{MSD}}{d\Omega d\in_b} = \frac{1}{4\pi}\frac{d\sigma_{MSD}}{d\in_b}\frac{2a}{e^a - e^{-a}}\exp(a\cos\theta) \tag{4.9}$$

where θ is the emission angle in the centre of mass system. According to the K-M systematics the slope parameter a of the exponential for incident energies below 80 MeV should to first order be a function only of the energy parameter, which is written as

$$e_b = \epsilon_b + B_b \tag{4.10}$$

where ϵ_b is the total kinetic energy in the exit channel and B_b is the binding energy of the emitted particle b in the composite nucleus. The angular distribution of the multistep compound (MSC) part is symmetric around 90^0 in the centre of mass. The multistep compound (MSC) part of the cross section is given by [Kal88]

$$\frac{d^2\sigma_{MSC}}{d\Omega d\,\epsilon_b} = \frac{1}{4\pi}\frac{d\sigma_{MSC}}{d\,\epsilon_b}\frac{a}{e^a - e^{-a}}\left[\exp(a\cos\theta) + \exp(-a\cos\theta\right]. \tag{4.11}$$

The general expression for the angular distribution in the centre of mass system is obtained by combining equation 4.9 and 4.11 and is given by [Kal88]:

$$\frac{d^2\sigma}{d\Omega d\,\epsilon_b} = \frac{1}{4\pi}\frac{d\sigma}{d\,\epsilon_b}\frac{a}{\sinh(a)}\left[\cosh(a\cos\theta) + f_{MSD}\sinh(a\cos\theta)\right] \tag{4.12}$$

where

$\epsilon_b \equiv$ is the emission energy

$\frac{d\sigma}{d\,\epsilon_b} \equiv$ is the angle integrated cross section of the emitted particle b

$f_{msd} \equiv$ is the fraction of the cross section due to a multistep direct (MSD) process

$\theta \equiv$ is the emission angle

$a \equiv$ is the slope parameter as defined in eq.4.7.

The angle integrated cross sections $\frac{d\sigma}{d\,\epsilon_b}$ are obtained either from preequilibrium model calculations or from the experiment. The list of parameters used to calculate the slope parameter a is given in Table 4.2.

Table 4. 2*: List of parameters and their values used to calculate the slope parameter a as defined in eq.4.7.*

Parameters	Value
n2	3
n3	4
C_1	0.04
C_2	1.8×10^{-6}
C_3	6.7×10^{-7}
E_{t1}	130
E_{t3}	41
M_p	1
m_α	2
$m_{He\text{-}3}$	1

A FORTRAN program was written to calculate the double differential cross sections in the center of mass according to equation 4.12 for the (p, α) and (p,^{3}He) reactions on ^{40}Ca at emission angles of 40.1^0 , 45.5^0 and 51.5^0 and emission energies from 1 to 100 MeV. The cross sections were calculated for f_{msd} = 1 which represents a 100% multistep direct process (MSD) contribution to the double differential cross sections. The angle integrated cross sections $\frac{d\sigma}{d\in_b}$ were calculated within the frame-work of the exciton model using the FORTRAN computer code PRECO-2000 which is described in the next section. The angle integrated cross sections $\frac{d\sigma}{d\in_b}$ were used to normalize the cross sections calculated with eq.4.12. These cross sections of the alpha and ^{3}He particles are shown at different emission energies in the center of mass system in figure 4.1. Because no full angular distributions were measured during the experiment the calculated values were used as multiplication factors to obtain the double differential cross sections for emitted alpha and ^{3}He, respectively.

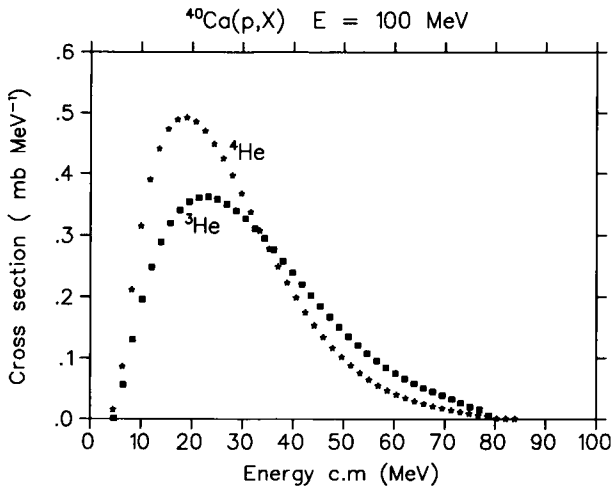

Figure 4.1: *The PRECO-2000 calculations of the c.m angle-integrated cross sections of the alpha and ^{3}He particles emitted in the reaction of 100 MeV protons on ^{40}Ca.*

The double differential cross sections were then converted from the center of mass to the laboratory system by dividing the calculated double differential cross sections from equation 4.12 by a relativistic jacobian. The corresponding emission energies were also converted to the laboratory system.

A two-body kinematic program was used in order to obtain the relationship of the relativistic jacobian, lab emission energy and centre of mass emission angle as a function of the centre of mass energy. These values were obtained over an angular range of 40^0 to 52^0 in 0.1^0 steps at excitation energies of 10 to 100 MeV in 10 MeV steps. The Table Curve program [SPS01] was used to fit the curves to these values in order to obtain the expressions to calculate the relativistic jacobian, the lab emission energy and the centre of mass emission angle as a function of the centre of mass energy. An example of the relativistic jacobian, lab energy and centre of mass angle as function of emission energy in the center of mass of an alpha particle emitted at the lab angle of 40^0 is shown in figures 4.2, 4.3 and 4.4, respectively. Similar fits were also obtained for alphas emitted at 45^0 and 51^0 as well as for the emission of ^{3}He particles at the same angles. The expressions for the relativistic jacobians, lab emission energies and centre of mass emission angles of alpha and ^{3}He particles at 40^0, 45^0 and 51^0 are summarized as follows:

(i) Relativistic jacobian

$$RJ=\frac{1}{\left(a_1+\frac{b_1}{\sqrt{\epsilon_b}}\right)} \tag{4.13}$$

where

RJ≡ relativistic jacobian

ϵ_b ≡ emission energy in the center of mass

a_1 ≡ see Table 4.3

b_1 ≡ see Table 4.3

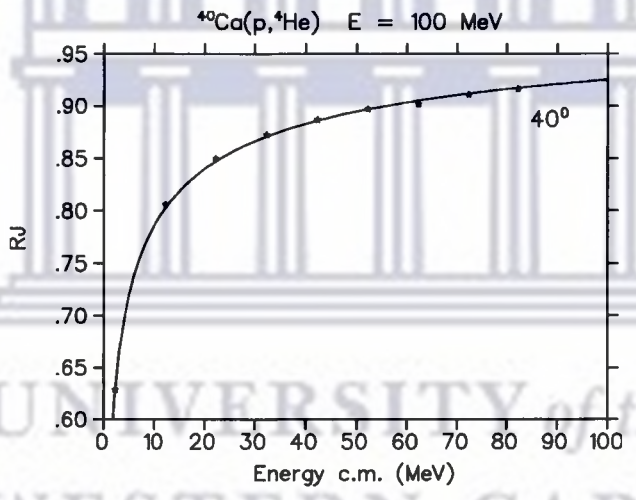

Figure 4.2: *Kinematic calculations of the relativistic jacobian (RJ) as a function of the centre of mass energy of the alphas emitted in the reaction of 100 MeV protons on ^{40}Ca at the laboratory emission angle of 40^0. The dots represent the kinematic calculations while the solid line represents the fit according to equation 4.13.*

(ii) Lab energy

$$E_{lab}=a_2+b_2\times\epsilon_b \tag{4.14}$$

where

E_{lab}≡ emission energy in the laboratory system

a_2 ≡ see Table 4.3

b_2 ≡ see Table 4.3

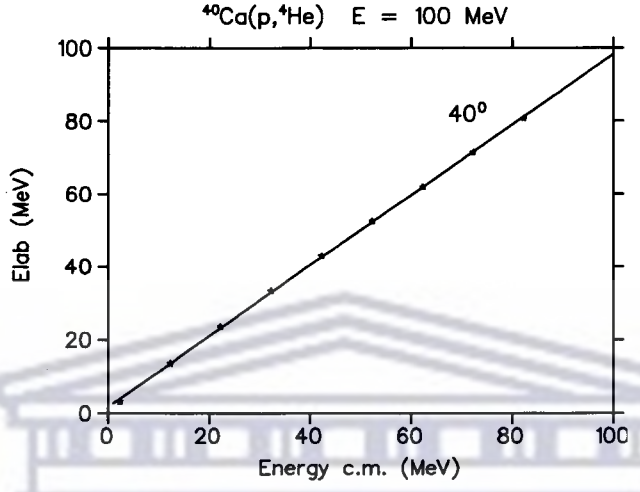

Figure 4.3: *Kinematic calculations of the lab emission energy as function of the centre of mass energy of the alphas emitted in the reaction of 100 MeV protons on ^{40}Ca at the laboratory emission angle of 40^0. The dots represent the kinematic calculations while the solid line represents the fit according to equation 4.14.*

(iii) Centre of mass angle

$$\theta_{cm} = a_3 + \frac{b_3}{\left(\sqrt{\epsilon_b}\right)} \tag{4.15}$$

where

θ_{cm} ≡ emission angle in the center of mass system

a_3 ≡ see Table 4.3

b_3 ≡ see Table 4.3

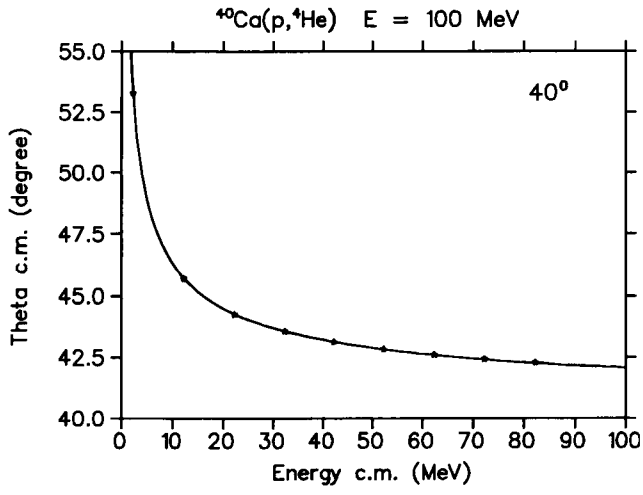

Figure 4.4: *Kinematic calculations of the centre of mass emission angle as function of the centre of mass energy of the alphas emitted from the reaction of 100 MeV protons on ^{40}Ca at the laboratory emission angle of 40^0. The dots represent the kinematic calculations while the solid line represents the fit according to equation 4.15.*

The list of the parameters together with their values for alpha and ^{3}He particle emission are listed in Table 4.3.

Table 4. 3: *List of parameters and their values used to calculate relativistic jacobians, lab emission energies and centre of mass emission angles for alpha and ^{3}He particles in equations 4.4, 4.5 and 4.6.*

Angles (degrees)	Parameters	Values for ^{4}He	Values for ^{3}He
40.1^0	a_1	0.99315856	0.99636724
	a_2	1.7287592	1.5329249
	a_3	40.103564	40.128438
	b_1	0.88176309	0.73684463
	b_2	0.966675	0.98428786
	b_3	19.65391	16.718613
45.5^0	a_1	0.99530777	0.9980429
	a_2	1.5401284	1.37368
	a_3	45.395971	45.428303
	b_1	0.79042132	0.6634906
	b_2	0.96137617	0.97948274
	b_3	21.777976	18.501366
51.5^0	a_1	0.99936136	1.0000629
	a_2	1.2925341	1.1767157
	a_3	51.809718	51.52719
	b_1	0.67632582	0.57211039
	b_2	0.95477467	0.97337964
	b_3	23.598616	20.360722

4.2 Calculations with PRECO-2000

PREC0-2000 is a computer code designed to study preequilibrium direct reactions [Kal05]. These calculations are based on the original work of Griffin [Gr66] which launched the field of preequilibrium reaction studies and led to the development of a whole host of models like the exciton model which were applied phenomenologically and quantum mechanically [Kal05]. These models describe the way in which the projectile energy slowly gets redistributed among the constituent nucleons of the composite system through a series of residual two-body interactions.

4.2.1 Exciton Model

In the exciton model the nucleus is assumed to have equally spaced single particle states. The states of the nucleus as a whole are described in terms of the number of particle and hole degrees of freedom which they contain. The interactions which cause transitions from one class of states to another are assumed to be two-body, residual and energy conserving in nature [Kal01]. The limitation of the two-body interaction is that it can only affect the energy conserving transition which changes the number of excitons by 0 or ±2 is raised and exploited to eliminate matrix elements which disappear identically [Gr66]. The factor of the two-body interaction is contained in order to show most simply the dependence of decay probability on the excitation energy of the composite nucleus and the excitation energy of the residual nucleus. Whenever the composite nucleus undergoes a transition to an intermediate state whereby one exciton has the energy in the continuum while the remaining exciton share the residual energy, a decay product is emitted with the exciton energy [Gri66].

This model has been successful in reproducing both the energy spectra of the emitted particles and the excitation functions for the formation of the specific product at incident energies, which typically range from 14 to 200 MeV for the reactions involving only nucleons in the entrance and exit channels [Kal05]. Examples are the (n,nx) reaction on ^{90}Zr at an incident energy of 14.1 MeV [Kon04] and the (p,xn) reaction on ^{90}Zr at an incident energy 80 and 160 MeV [Chad94].

4.2.2 Application of Exciton Model in PRECO-2000

Kalbach has modified and compared exciton model calculations with experimental energy spectra from inclusive (nucleon, nucleon) reactions at energies of 14 to 25 MeV. The initial target–projectile interaction in (nucleon, nucleon) reactions indicated that the model formulation works well up to incident energies of around 25 MeV [Kal05]. For example the (n,xp) reaction on ^{27}Al at an incident energy of 14.8 MeV and the (n,xn) reaction on ^{40}Ca at an incident energy of 14.1 MeV [Kal98] have been studied.

The phenomenological models used to describe direct nucleon transfer processes and reactions involving cluster degrees of freedom were first developed in 1977 [Kal77] and later modified for use in PRECO-D2 [Kal05]. The models in the code give a phenomenological statistical description of the direct transfer of one or more nucleons (stripping and pickup) and of direct knockout and inelastic scattering involving cluster degrees of freedom.

Nuclear transfer is the primary mechanism needed to supplement the exciton model in nucleon-induced reactions. It also plays a significant role in reactions with complex projectiles. In the reaction A (a, b) B, the energy differential cross section for nuclear transfer (pickup, stripping or nucleon exchange) is given by [Kal2005]

$$\left[\frac{d\sigma_{a,b}(\varepsilon)}{d\varepsilon}\right]=\frac{2s_b+1}{2s_a+1}\frac{A_b}{A_a}\frac{\varepsilon\sigma_b(\varepsilon)}{A_a}K_{\alpha,p}\left(\frac{A_a}{E_a+V_a}\right)^{2n}\times\left(\frac{2860}{A_A}\right)^{n}\frac{1}{80\varepsilon_a}\sum_{p_\pi}\left(\frac{2Z_A}{A_A}\right)^{6n_\pi}\omega(p_\pi,h_\pi,p_\nu,h_\nu,U) \tag{4.16}$$

where

N, Z, and A are the neutron, proton and the mass numbers of the nucleus designated by its subscripts

s ≡ spin of the designated particle

ε_a ≡ energy variable for the entrance channel energy

ε ≡ energy variable for the exit channel energy

E_a ≡ energy variable for the projectile laboratory energy

$\sigma_b(\varepsilon)$ ≡ gives the exit channel total nonelastic cross section

p_π, h_π, p_ν and h_ν ≡ number of proton particles, proton-hole, neutron-particles and neutron-hole degrees of freedom in the residual nucleus

$n = p_\pi + h_\pi + p_\nu + h_\nu$ ≡ total number of excitons or degrees of freedom

$n_\pi = p_\pi + h_\pi$ ≡ number of proton degrees of freedom

$\omega(p_\pi, h_\pi, p_\nu, h_\nu, U)$ ≡ density of the residual states at excitation energy U.

The constant $K_{\alpha,p}$ provides an enhancement factor of 12 for (N,α) and (α,N)reactions, where both projectile and ejectile are tightly bound. The quantity V_a is the empirical energy of (12.5 MeV $\times A_a$) which represents the energy difference experienced by the projectile to the Fermi level of the nucleus. The energies are in MeV and the cross sections are in mb.

4.2.3 ^{40}Ca (p, α) and ^{40}Ca (p, ^{3}He) Calculations

PRECO-2000, also known as PRECOM is a two-component exciton model code for the calculation of double differential cross sections of light particle nuclear reactions [Kal2005]. PRECO-2000 calculates the emission of light particles (A = 1 to 4) from nuclear reactions induced by light particles on a wide variety of target nuclei. Their distributions as function of both energy and angle are calculated. The PRECO-2000 code is written in FORTRAN and was used in the present study to calculate the double differential cross sections of the emitted alpha and ^{3}He particles.

Input files were created in order to calculate both differential energy as well as the double differential cross sections of the emitted alpha and ^{3}He particles in the centre of mass system. The input file and the input parameters together with their values are shown in appendix A.

The PRECO-2000 calculations were performed from 0^0 to 180^0 in the centre of mass system. Since the calculations performed with PRECO-2000 are expressed in the center of mass the calculated double differential cross sections were converted to the laboratory system as described in the previous section. Comparisons with the experimental cross sections were performed for the two laboratory emission angles of 40^0 and 50^0.

CHAPTER 5 Results

5.1 Overview

This chapter presents the experimental results of the inclusive spectra of the $^{40}Ca(p,\alpha)$ and $^{40}Ca(p,^{3}He)$ reactions in the form of double differential cross sections which were produced from the prescaled-singles data. These data are compared with theoretical predictions, which are described in the previous chapter. The measured double differential cross section spectra were compared to the calculated angular distributions based on the Kalbach systematics as well as the exciton model preequilibrium code PRECO-2000.

5.2 Inclusive spectra of ^{3}He and ^{4}He

In the $^{40}Ca(\vec{p},p'\alpha)^{36}Ar$ reaction the incident polarized proton knocks out an alpha particle, which is bound in the ^{40}Ca target, to produce three reaction products in the final state. These are the scattered proton p', the knocked out alpha particle and the residual nucleus ^{36}Ar. In order to study alpha clustering in ^{40}Ca with this quasi-free knockout reaction at an incident energy of 100 MeV, both the analyzing powers as well as double differential cross sections were measured. Coincidence data between the alpha particles and the scattered protons were measured at the quasi-free angle pairs of (θ_{K600}, $\theta_{telescope}$) = (59^0, -51.5^0), (70^0, -45.5^0) and (81^0, -40.1^0). As part of the data analysis the consistency of each detector had to be checked individually. In order to perform this requiment for the alpha-particle telescope, double differential cross sections of the ^{3}He and ^{4}He particles were extracted from the prescaled singles data set at the emission angles of 40.1^0, 45.5^0 and 51.5^0. These double differential cross sections are shown in figures 5.1 and 5.2, respectively. Due to the detector characteristics and energy thresholds, these continuum cross sections were measured between emission energies of about 12 to 66 MeV excluding any discrete states.

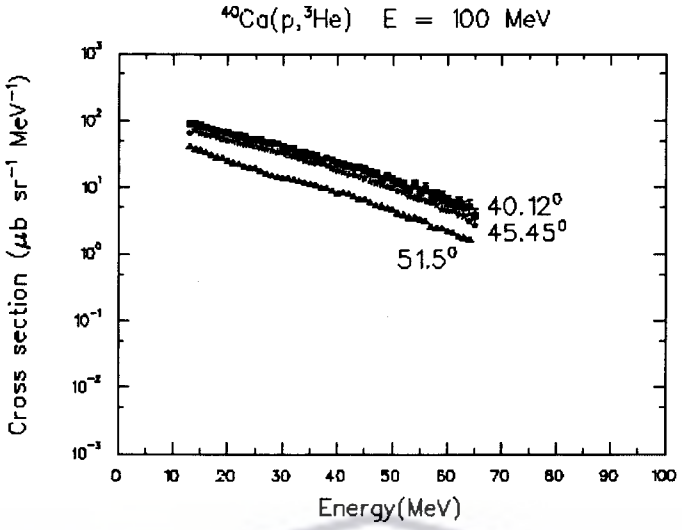

Figure 5. 1: *Double differential cross sections of the ^{3}He particles emitted from the reaction of 100 MeV protons on ^{40}Ca at different emission angles as indicated. The error bars show the statistical error where these exceed the symbol size.*

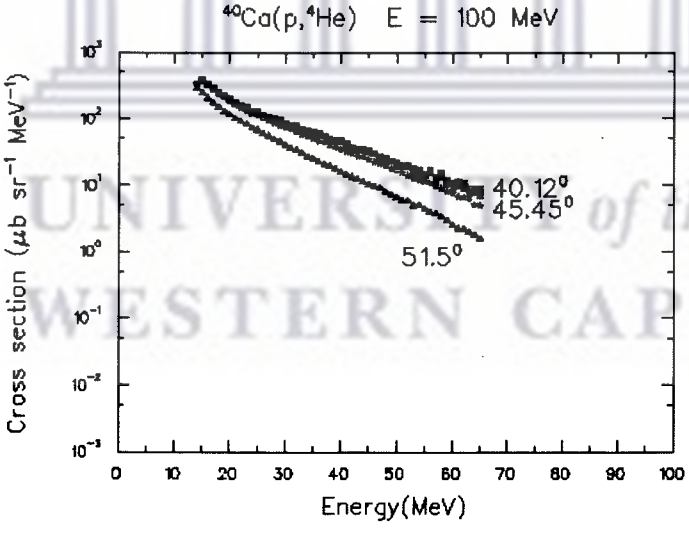

Figure 5. 2: *Double differential cross sections of the alpha particles emitted from the reaction of 100 MeV protons on ^{40}Ca at different emission angles as indicated. The error bars show the statistical error where these exceed the symbol size.*

In order to check the accuracy of the present data, the spectra were compared with a previous measurement [Wu79]. The experimental double differential energy cross sections at the emission angle of 45.45^0 were compared with the spectra for ^{3}He and α particles for 100 MeV proton induced reactions on ^{58}Ni [Wu79] as shown in figure 5.3 and figure 5.4, respectively. The ^{58}Ni data were chosen since the present cross sections on ^{40}Ca data were never measured before. The present measurements agree well both qualitatively and quantitatively with the ^{58}Ni data. This comparison thereby confirms that the efficiency of the silicon detector telescope is accurate.

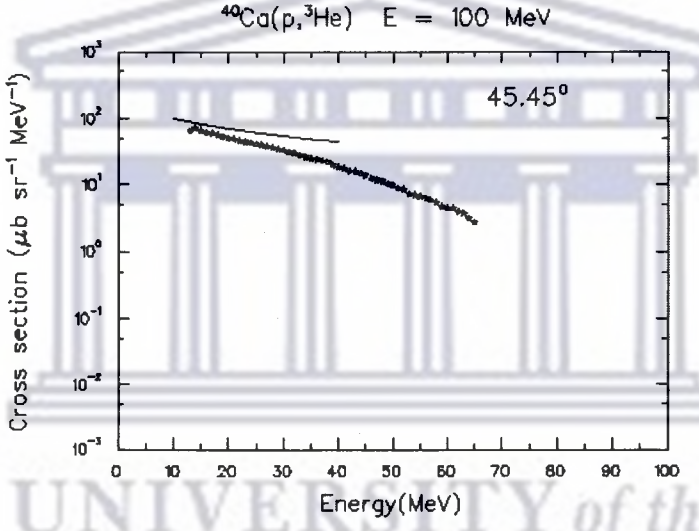

Figure 5. 3: *Double differential cross sections of the ^{3}He particles emitted from the reaction of 100 MeV protons on ^{40}Ca at 45.4^0, compared with the ^{58}Ni data of Wu et al. [Wu79], which are shown as the curve. The error bars show the statistical error where these exceed the symbol size. The systematic uncertainties of the ^{58}Ni data of Wu et al. [Wu79] is 10 % whereas for the double differential cross sections of the ^{3}He particles emitted from the reaction of 100 MeV protons on ^{40}Ca at 45.4^0 is 5.5%.*

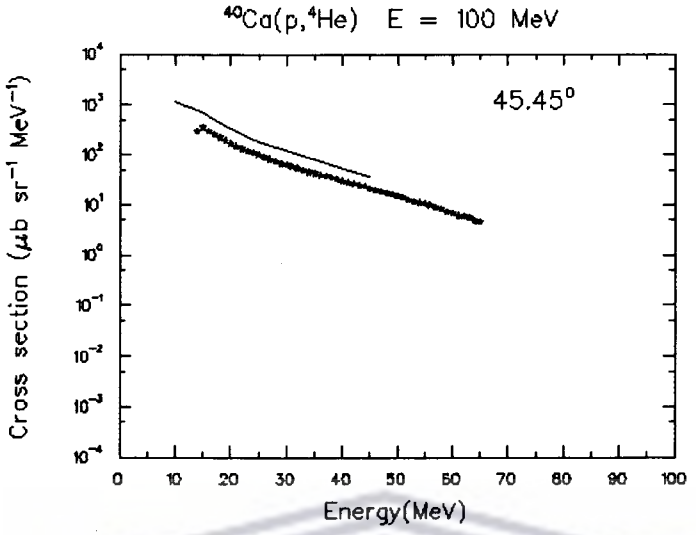

Figure 5. 4: *Double differential cross sections of the ^{4}He particles emitted from the reaction of 100 MeV protons on ^{40}Ca at 45.4^{0}, compared with the ^{58}Ni data of Wu et al. [Wu79], which are shown as the curve. The error bars show the statistical error where these exceed the symbol size. The systematic uncertainties of the ^{58}Ni data of Wu et al. [Wu79] is 10 % whereas for the double differential cross sections of the ^{4}He particles emitted from the reaction of 100 MeV protons on ^{40}Ca at 45.4^{0} is 5.5%.*

Figure 5.5 represents the inclusive spectra for ^{3}He and ^{4}He at 40.1^{0} from 100 MeV protons incident on ^{40}Ca. The double differential cross sections for ^{4}He are found to be larger than for ^{3}He particle because the alpha particle is much stronger bound than the ^{3}He particle. The binding energy of ^{3}He is 6.98 MeV whereas for the alpha particle it is 20.58 MeV. The spectra show similar exponential shapes for both the (p, ^{3}He) and (p, ^{4}He) reactions as shown in figure 5.5. There are more lower energy alphas than ^{3}He particles, probably because the preformation probability is likely to be larger for alphas than for ^{3}He particles in ^{40}Ca.

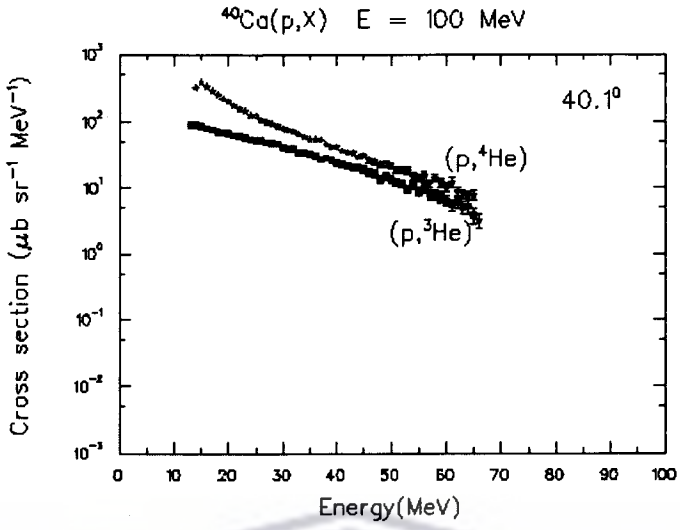

Figure 5. 5: *Double differential cross sections of the ^{3}He and ^{4}He particles emitted from the reaction of 100 MeV protons on ^{40}Ca at 40.1^0. The error bars show the statistical error where these exceed the symbol size.*

5.3 Model calculations

The experimental double differential cross sections of the ^{3}He and ^{4}He particles emitted at lab angles of 40.1^0 and 51.5^0 were compared to double differential cross section calculations based on the Kalbach systematic parameterization [Kal88] as well as the PRECO-2000 exciton model code [Kal2005]. The comparisons are shown in figures 5.6 and 5.7 for the emission of ^{3}He particles. For the emitted ^{4}He particles, the comparisons are shown in figures 5.8 and 5.9. The comparison of the Kalbach systematics and the PRECO-2000 calculations are shown as a function of the emission energies. These calculations are fundamentally different since the Kalbach systematics is a purely phenomenological description while the PRECO-2000 code is based on the nuclear exciton model.

5.3.1 Kalbach Parameterization

For the (p, ^{4}He) reaction the Kalbach calculations agree qualitatively with the experimental results seen figures 5.8 and 5.9. However, there is some discrepancy for the cross sections at emission energies of less than 25 MeV. In this energy region in which the phenomenological prescription tends to underpredict the experimental data it is speculated that these features in the experimental data are related to an evaporation mechanism, not accounted for by the phenomenological prescription.

In the case of the (p, ^{3}He) reaction cross sections the phenomenological prescription of Kalbach overpredicts the data (See figs 5.6 and 5.7) while for the (p, ^{4}He) reaction itb tend to be more consistent with the data (See figs 5.8 and 5.9). This discrepancy with the experimental data is also related to the way the parameterized cross sections had to be normalized. As discussed in chapter 4 the phenomenological prescription of Kalbach cross sections were normalized with the angle integrated cross sections $\frac{d\sigma}{d\in_b}$, which were calculated within the framework of the exciton model usingcomputer code PRECO-2000. The Kalbach results confirm that for a bombarding energy of 100 MeV or less the main physical parameter, which determines the shape of the angular distribution, is the energy of the emitted particle. From results obtained from inclusive spectra of the $^{40}Ca(p,\alpha)$ and $^{40}Ca(p,^3He)$ reactions with 100 MeV protons it can be concluded that the reaction mechanism can be interpreted to a large extent in terms of a multistep direct process which supports the qualitative conclusions made in earlier studies.

These studies made use of similar calculations with the Kalbach systematics for the cross sections of the inclusive (p, α) and (p, ^{3}He) reactions on ^{27}Al, ^{59}Co and ^{197}Au at incident energies between 120 and 200 MeV [Cow96, Cow97]. The experimental angular distributions between 10^0 and 160^0 were compared with the prediction of the phenomenological parametrization of Kalbach [Kal80]. It was found that the shape of the experimental (p, α) and (p, ^{3}He) distributions are reproduced reasonably well by the predictions of the Kalbach parametrization. As the incident energy increases the predicted curves deviated slightly from the measured distributions. At forward angles

Kalbach underpredicts the data whereas at backward angles it overpredicts the data. Similarly to ^{27}Al and ^{59}Co which are light target nuclei the present study on ^{40}Ca was to establish whether the double differential cross sections can be analysed in terms of a multistep direct (MSD) process and in which way the multistep compound (MSC) process contributes to the cross sections. It can be concluded that the inclusive spectra of the $^{40}Ca(p,\alpha)$ reaction can be analyzed successfully in terms of the Kalbach systematics except in the low energy region where other mechanisms like evaporation for example will contributes.

5.3.2 Exciton Model

In the present study exciton model calculations were performed for the cross sections of the inclusive (p, α) and (p, ^{3}He) reactions on ^{40}Ca at an incident energy of 100 MeV. The nuclear exciton model for (p, α) (See figs 5.8 and 5.9) reaction agree well with the experimental data while for (p, ^{3}He) reaction overpredicts the data (See figs 5.6 and 5.7). The spectra show some slight overestimation of the cross sections at large emission energies.

For the (p, ^{4}He) reaction the theory agrees qualitatively with the experimental results. However there is some discrepancy for the cross sections at an emission energy of less than 25 MeV. In this energy region in which nuclear exciton models tends to underpredict the experimental data it is speculated that these features are related to an evaporation mechanism, not accounted for by the nuclear exciton model. The spectra show some overestimation of the cross sections at the higher emission energies.

For the (p, ^{3}He) reaction the PRECO-2000 model underpredicts the slope of the data while for (p, ^{4}He) the PRECO-2000 model tends to be roughly consistent but for emission energy between 30 and 50 MeV the calculated curves lie above the experimental cross sections. It can be concluded that the inclusive spectra of the $^{40}Ca(p,\alpha)$ and $^{40}Ca(p,^3He)$ reactions can be analyzed successfully in terms of the nuclear exciton model except in the low energy region where the evaporation mechanism contributes.

In a comparative study complete light charged particle ($Z \leq 2$, $A \leq 4$) spectra were measured for 90 MeV protons on ^{27}Al, ^{58}Ni, ^{90}Zr and ^{209}Bi and 100 MeV protons on ^{58}Ni [Wu79]. The results show that spectra of each emitted light charged particle has a characteristic behavior with angle, which is similar for all target nuclei except in the low energy evaporation region. The high-energy continuum region of the spectra show a strong angular dependence in the forward direction suggesting that this region is dominated by direct reactions. The proton and alpha spectra in the backward directions and at low energies are nearly isotropic especially for the lighter nuclei, which indicates that the region is dominated by an equilibrium process [Wu79]. The shape of the deuteron spectra is very similar to the spectra of protons [Wu79]. It was concluded that the reaction mechanism of protons and deuterons are similar in the high energy region for all target nuclei. In the backward direction ($\theta \geq 140^0$) the spectra exhibit characteristic evaporation behavior with approximately the same slope for each target nucleus for a given observed particle. The slopes of the evaporation peaks for different particle types are also similar. These experimental results were analyzed within the framework of the preequilibrium exciton model as well as evaporation model [Wu79]. The comparisons of the experimental results with these calculations indicate that multistep collisions are significant in this energy range particularly for complex particle emission [Wu79]. The ^3He and alpha energy spectra are reasonably well reproduced by the preequilibrium exciton model. It was found that for heavy nuclei the preequilibrium reaction dominates the cross sections for ^{3} He and alpha particle emission.

The reactions involving cluster degrees of freedom occur when a complex projectile excites a neutron, proton or alpha particle-hole pair while retaining its cluster identity or when a nucleon projectile excites an alpha particle-hole pair. Each of these interactions form a three-exciton or two-particle one-hole state, which decay by emission of one or the other particle degree of freedom [Kal05].

The exciton model results of [Wu79] differ from the present study since only angle intergrated cross sections could be described by the exciton model calculations. The code PRECO-2000 [Kal05] on the other hand is able to calculate double differential cross sections as function of emission energy as well as angle. This has to be seen as a

necessary improvement in the way the exciton model is applied in performing calculations of complex particle emission to the continuum. For ^{3}He and alpha energy spectra it was found that the single step and multistep direct mechanism are necessary. It was found that the reaction mechanism for the emission of ^{3}He can be linked to deuteron pickup whereas for the emission of ^{4}He is quasifree knockout as the last step.

In a separate project, conducted also as part of this experiment, the analyzing powers for the inclusive $(\vec{p},\alpha)$ and $(\vec{p},^3He)$ reactions on ^{40}Ca with 100 MeV polarized protons were studied at the same emission angles of 40.1^0, 45.5^0 and 51.5^0. Comparisons with previous findings indicate that the present results are in good agreement with each other and are consistent with previous results. It was found that the analyzing powers seem to be guided by the single step at high alpha and ^{3}He emission energies where relatively large analyzing powers were measured. This seems to suggest that a single step or very few steps contribute to non-zero $(\vec{p},\alpha)$ and $(\vec{p},^3He)$ continuum analyzing powers. As the emission energy decreases the continuum analyzing power approaches a value of zero which previously also was associated with multistep process describing a chain of nucleon-nucleon interactions inside the composite nucleus with the eventual emission of ^{3}He or ^{4}He particle to the continuum as the final step. These results strengthen the present interpretation that inclusive continuum spectra of the $^{40}Ca(p,\alpha)$ and $^{40}Ca(p,^3He)$ reactions can be analysed successfully in terms of the nuclear exciton model based on single step and multistep mechanism. It was found that the reaction mechanism for the emission of ^{3}He can be linked to deuteron pickup whereas for the emission of ^{4}He is quasiefree knockout describing a chain of nucleon-nucleon interactions inside the composite nucleus with the eventual emission of ^{3}He or ^{4}He particle to the continuum as the last step.

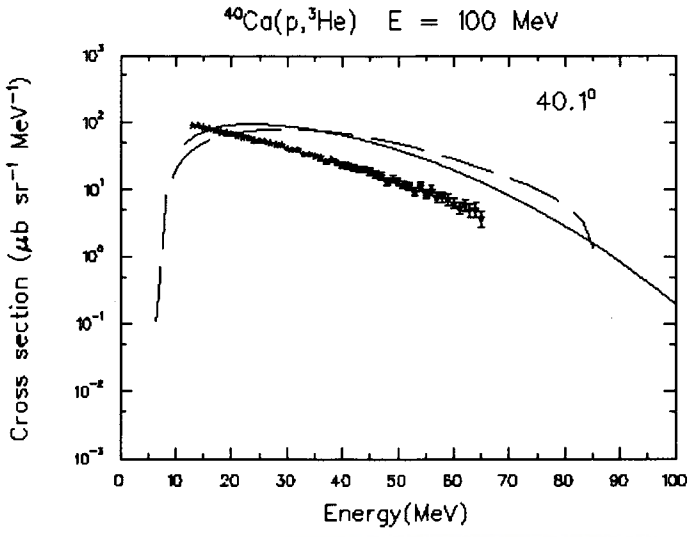

Figure 5. 6: *Comparisons of the experimental double differential cross sections of ^{3}He particles emitted from the reaction of 100 MeV protons on ^{40}Ca at a laboratory emission angle of 40.1^{0} with calculations based on the Kalbach systematics and the PRECO-2000 code. The solid curve represents the calculation with the Kalbach systematics and the dashed curve is the PRECO-2000 calculations. The error bars show the statistical error where these exceed the symbol size.*

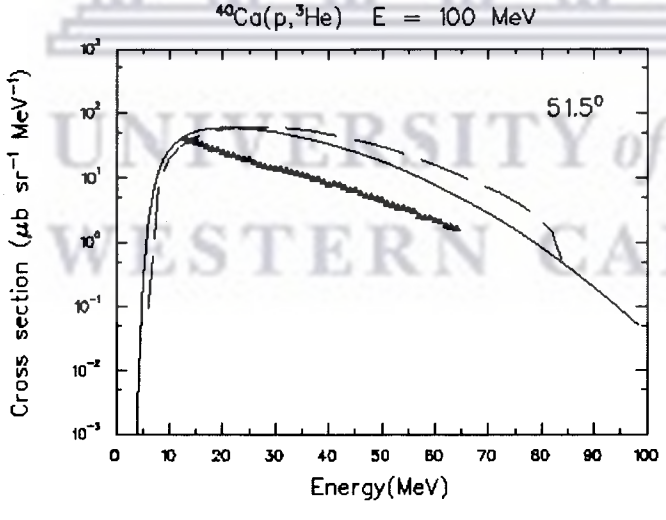

Figure 5. 7: *Comparisons of the experimental double differential cross sections of ^{3}He particles emitted from the reaction of 100 MeV protons on ^{40}Ca at a laboratory emission angle of 51.5^{0} with calculations based on the Kalbach systematics and PRECO-2000 code. The solid curve represents the calculation with the Kalbach systematics and the dashed curve is the PRECO-2000 calculations. The symbols are the experimental data.*

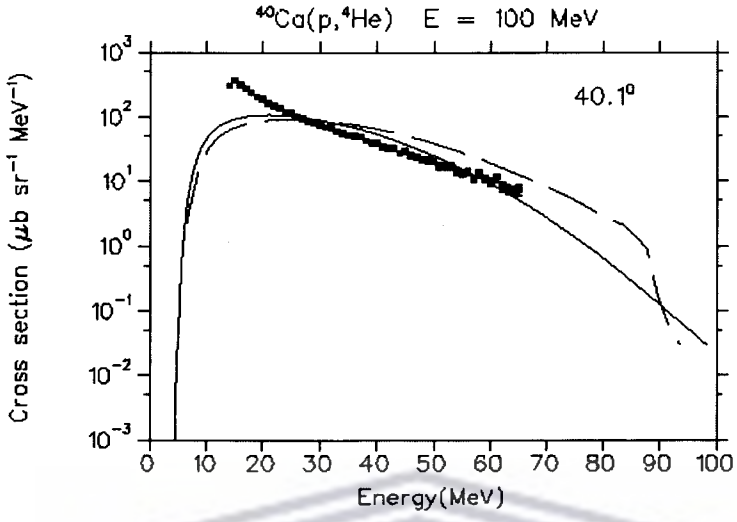

Figure 5. 8: *Comparisons of the double differential cross sections of ^{4}He particles emitted from the reaction of 100 MeV protons on ^{40}Ca at a laboratory emission angle of 40.1^{0} with calculations based on the Kalbach systematics and the PRECO-2000 code. The solid curve represents the calculation with the Kalbach systematics and the dashed curve is the PRECO-2000 calculations. The error bars show the statistical error where these exceed the symbol size.*

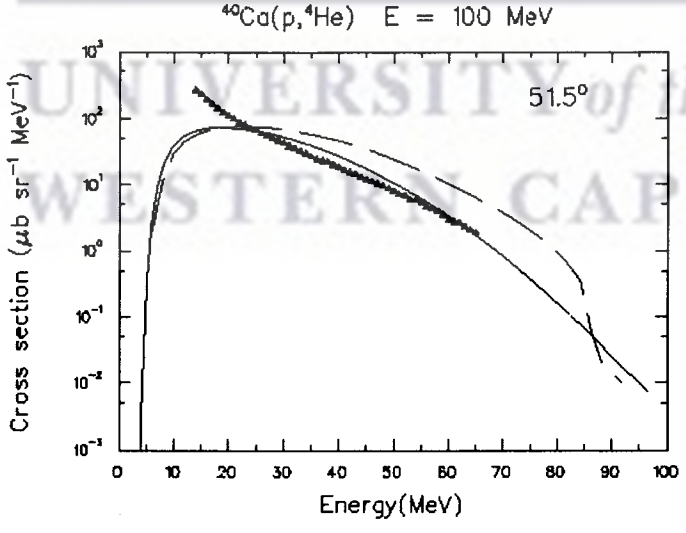

Figure 5. 9: *Comparisons of the double differential cross sections spectra of ^{4}He particles emitted from the reaction of 100 MeV protons on ^{40}Ca at a laboratory emission angle of 51.5^{0} with calculations based on the Kalbach systematics and the PRECO-2000 code. The solid curve represents the calculations with the Kalbach systematics and the dashed curve is the PRECO-2000 calculations. The symbols are the experimental data.*

CHAPTER 6 SUMMARY AND CONCLUSIONS

The aim of the coincidence experiment was to study alpha clustering in ^{40}Ca with the $^{40}Ca(\vec{p}, p\alpha)$ quasifree knockout reaction at incident energy of 100 MeV. Coincidence analyzing power and cross section data were measured at the quasifree angle pairs of (θ_{K600}, $\theta_{telescope}$) = (59^0, -51.5^0), (70^0, -45.5^0) and (81^0, -40.1^0). The present study therefore had the following two aims. The first was to test the efficiency of the silicon detector telescope, which was used to detect the alpha particles. The second was to extract double differential cross sections of the emitted ^{3}He and ^{4}He particles from the prescaled singles data set at the selected angles of 40.1^0, 45.5^0 and 51.5^0 and to test these against preequilibrium model calculations.

In order to test the efficiency of the detector telescope the experimental double differential cross sections were overlayed onto the existing data of the $^{58}Ni(p,\alpha)$ and $^{58}Ni(p,^3He)$ reactions measured at 100 MeV incident energy and at an emission angle of 45^0. The present results are found to be consistent with the previous data thereby confirming the efficiency of the silicon detector telescope.

Overall the continuum $(p,^3He)$ cross sections were found to be about five times smaller than the (p,α) cross sections mainly because the alpha particle is stronger bound than the ^{3}He particle. The double differential (p,α) and $(p,^3He)$ cross sections at the emission energies of 12 to 66 MeV were fitted with the Kalbach parameterization. From the results obtained from the inclusive spectra of the $^{40}Ca(p,\alpha)$ and $^{40}Ca(p,^3He)$ reactions with 100 MeV protons it is concluded that the reaction mechanism can be interpreted to a large extent in terms of a multistep direct process.

The preequilibrium exciton model was used to calculate the continuum (p,α) and $(p,^3He)$ cross sections at lab angles of 40.1^0 and 51.5^0.The preequilibrium exciton model reproduced the experimental energy spectra reasonably well both in shape as

well in magnitude. The preequilibrium exciton model analyzed continuum (p, α) and (p, ^{3}He) spectra successfully except in the low energy region where the evaporation mechanism contributes. From the theoretical treatment of the (p, α) and (p, ^{3}He) double differential cross sections, it can be concluded that the spectra can be reproduced in terms of a multi-step mechanism.

The reasonable agreement between the preequilibrium exciton model and the experimental (p, α) and (p, ^{3}He) cross sections supports the multistep character of the reaction mechanism. Pre-equilibrium emission of ^{3}He and ^{4}He particles takes place from a composite nucleus which is formed after the projectile-target nucleus interaction .This interaction is described in terms of successive two-body residual interactions leaving excited nucleons in intermediate states. In the exciton model complex particles like ^{3}He and ^{4}He are then treated as clusters of these excited nucleons which consequently decay as excitons to the continuum. Furthermore this study has shown that the exciton model as applied in the PRECO-2000 code is able to calculate double differential cross sections of complex particle emission to the continuum. Previously the exciton model was restricted in its predictive power to differential cross sections.

In addition to cross sections the continuum analyzing powers are known to help to distinguish between different possible mechanisms as for example transfer and knockout. The $(\vec{p},^3He)$ and $(\vec{p},\alpha)$ continuum analyzing powers provide therefore stringent tests of the inferred reaction mechanisms which would complement the findings of this study.

Appendix A

The input parameters that were used to calculate both differential energy as well as the double differential cross sections of the emitted alpha and ^{3}He particles in the centre of mass system are described in this section.

(1) Title card

^{40}Ca+p at 100 MeV

(2) E, B_a

where

E ≡ excitation energy in MeV of composite nucleus ^{41}Sc

B_a≡ binding energy of the projectile in the composite nucleus ^{41}Sc in MeV

(3) Z_{tar}, N_{tar}

where

Z_{tar} ≡ proton number of the ^{40}Ca target

N_{tar} ≡ neutron number of ^{40}Ca target

(4) Z_a, N_a

Z_a ≡ proton number of the projectile

N_a ≡ neutron number of the projectile

6) B_n, B_p, B_d, B_t, $B_{He\text{-}3}$, B_{alpha}

where

B_n, B_p, B_d, B_t, $B_{He\text{-}3}$, B_α is the binding energy in MeV of neutron, proton, deuteron, triton, helium-3 and alpha particles respectively in the composite nucleus ^{41}Sc.

(7) B_n (Z, N-1), B_p (Z, N-1), B_n (Z-1, N), B_p (Z-1, N)

neutron and proton binding energies in the residual nuclei following primary emission of neutrons and protons.

(8)K_{ang}, K_n, K_p, K_d, K_t, $K_{He\text{-}3}$, K_α

Output control variable for the emitted particle. For K_{ang}=1 double differential cross section to be calculated following the energy spectra for the particle types requested.

A value of K_b=1 causes the energy spectra for particle of type b to be printed while a value of zero suppresses printing.

Table A.1: *List of input parameters and their values used to calculate the double differential cross sections with PRECO-2000.*

Parameter	Value
E	100.7 MeV
B_a	1.08 MeV
Z_{tar}	20
N_{tar}	20
Z_a	1
N_a	0
B_n	16.19 MeV
B_p	1.08 MeV
B_d	14.5 MeV
B_t	21.53 MeV
B_{He-3}	14.77 MeV
B_{alpha}	6.27 MeV
B_n (Z, N-1)	14.42 MeV
B_p (Z, N-1)	0.54 MeV
B_n (Z-1, N)	15.64 MeV
B_p (Z-1, N)	8.33 MeV
K_{ang}	1

REFERENCES

[Bac73] D. Bachelier, M. Bernas, O.M. Bilaniuk, J.L. Boyard, J.C Jourdan and P. Ranvanyi, Phys. Rev. C 7, 165 (1973).

[Bon89] R. Bonetti and F. Crespi, Nucl. Phys. A 499, 381(1989).

[Car84] T.A. Carey, P.G. Roos, N.S. Chant, A. Nadasen and H.L. Chen, Phys. Rev. C 29, 1273 (1984).

[Cha94] M.B. Chadwick, P. G. Young, D. C. George, and Y. Watanabe, Phys. Rev. C 50, 996 (1994).

[Chi76] N. Chirapatpimor, Nucl. Phys. A 264, 379 (1976).

[Chu94] J.L. Chuma. PHYSICA Programme. *Reference Manual*, (1994).

[Cow90] A.A. Cowley, S.V. Förtsch, J.J. Lawrie, D.M.Whittal, F.D. Smit, and J.V. Pilcher, Z.Phys, A 336, 189 (1990).

[Cow91] A.A. Cowley, A.van Kent, J.J.Lawrie, S.V.Förtsch, D.M.Whittal, J.V.Pilcher and F.D.Smit, Phys. Rev. C 43, 678 (1991).

[Cow94] A.A.Cowley, G.F.Steyn, S.V. Förtsch, J.J.Lawrie, J.V.Pilcher, F.D.Smit, and D.M.Whittal, Phys. Rev. C 50, 2449 (1994).

[Cow96] A.A. Cowley, G.J. Arendse, J.W. Koen, W.A. Richer, J.A. Stander, Phys. Rev. C 54, 778 (1996).

[Cow97] A.A.Cowley, G.J. Arendse, G.F. Steyn, J.A. Stander, W.A. Richer, S.S. Dimitrova, P. Demetriou and P.E. Hodgson , Phys. Rev. C 55 , 1843 (1997).

[Cow00] A.A. Cowley, G.F. Steyn, S.S. Dimitrova, P.E. Hodgson, G.J. Arendse, S.V. Förtsch, G.C. Hillhouse, J.J. Lawrie, R. Neveling, W.A. Richter, J.A.S tander and S.M. Wyngaardt, Phys. Rev. C 62, 064605-1 (2000).

[Cow02] A.A. Cowley, S.V. Förtsch, G.F. Steyn, S. Dimitrova and P.E. Hodgson, Nucl. Science and Technology, 742 (2002).

[Fes80] H. Feshbach, A. Kerman and S. Koonin, *Ann. of Phys.* 125 (1980).

[Fes92] H. Feshbach, Theoretical Nuclear Physics, John Wiley and sons, New York, (1992).

[Fes95] H. Feshbach, Nucl. Phys. News, Vol.5, No.1, (1995).

[För06] S.V. Förtsch, Private communication.

[Gad92] E. Gadioli, and P. E. Hodgson, Pre-Equilibrium Nuclear Reaction, (Clarendon Press, Oxford, 1992).

[Gre82] R.E.L. Green, K.P. Jackson, and R.G. Korteling, Phys. Rev. C 25, 828 (1982).

[Gri66] J.J. Griffin, Phys. Rev. Lett. 17. 478 (1966).

[Hod93] P.E. Hodgson, Z. Phys. A349. 197 (1993).

[Iga] M. Igarashi, Tokyo Medical College, unpublished.

[Jip84] P. Jipsen, ELOSS, A programm for Calculating The RANGES OF IONS IN MATTER, National Accelerator Centre (1984) (unpublished).

[Kal77] C. Kalbach, Z. Phys. A 283, 401 (1977).

[Kal80] C. Kalbach, Phys. Rev. C 37, 2350 (1980).

[Kal81] C. Kalbach, Phys. Rev. C 23, 124 (1981).

[Kal83] A.M. Kalend, B.D. Anderson, A.R. Baldwin, R. Madey and J.W. Watson. Phys. Rev. C 28, 105 (1983).

[Kal88] C. Kalbach, Phys. Rev. C 37, 2350 (1988).

[Kal98] C. Kalbach, J. Phys. G: Nucl. Part. Phys. 24, 847 (1998).

[Kal01] C. Kalbach Exciton model preequilibrium code with direct reactions.

[Kal05] C. Kalbach. Phys. Rev. C 71, 034606-1 (2005).

[Kon04] A. J. Koning and M. C. Duijvenstijn, Nucl. Phys. A 744, 15 (2004).

[Kun] P.D. Kunz, University of Colorado, unpublished.

[Lew82] Z. Lewandowski, E. Loeffler and R.Wagner, Nucl. Phys. A 389, 247 (1982).

[Leo87] W.R. Leo, Techniques for Nuclear and Particle Physics Experiments, Springer-Verlag Berlin Heidelberg, (1987).

[Nad80] A. Nadasen, N.S. Chant, P.G. Roos, T.A. Carey, R. Cowen, C. Samanta and J.Wesick, Phys. Rev. C 22 , 1394 (1980).

[Nad81] A. Nadasen , P.G. Roos, N.S. Chant, A.A. Cowley, C. Samanta and J. Wesick, Phys. Rev. C 23 , 2353 (1981).

[Nad89] A. Nadasen, Phys. Rev. C 40 , 1130 (1989).

[Nad93] A. Nadasen, *ibid.* 47, 674 (1993).

[Nad99] A. Nadasen , J. Brusoe, J. Farhat, K.A.G. Rao, D. Sisan and J. Williams, Phys. Rev. C 59, 760 (1999).

[Pil89] J. V. Pilcher, Ph.D. thesis, University of Cape Town, (1989) (unpublished).

[Pil96] J. V. Pilcher, The NAC MBD to VME Conversion Guide (1996).

[Ray82] E.L. Ray. Green, K. Peter Jackson and Ralph G. Korteling, Phys. Rev. C 25, 828 (1982).

[Ren91] E. Renshaw, S.J. Yennello, K. Kwiatkowski, R. Planeta, L.W. Woo, and V.E. Viola, Phys. Rev. C 44, 2618 (1991).

[Roo77] P.G. Roos, N.S. Chant, A.A. Cowley, D.A. Goldberg, H.D. Holmgren and R. Woody, Phys. Rev. C 15, 69 (1977).

[Sak80] H. Sakai, K. Hosono, N. Matsuoka and S. Nagamachi, Nucl. Phys. A 344, 41 (1980).

[Sch71] P. Schwandt, T.B. Clegg, W. Haeberli, Nucl. Phys. A 163, 432 (1971).

[Scob90] W. Scobel, M. Trabandt, M. Blann, B.A. Pohl, B.R. Remington, R.C. Byrd, C.C. Foster, R. Bonetti, C. Chiesa, and S.M. Grimes, Phys. Rev. C 41, 2010 (1990).

[She76] J.D. Sherman, D.L. Hendrie and M.S Zisman, Phys. Rev. C 13, 20 (1976).

[SPS01] Table Curve 2D Version 5.1 SYSTAT Software, Marketed by: SPSS Inc. USA (2001).

[Ste99] G.F. Steyn, S.V. Förtsch, A.A. Cowley, J.J. Lawrie, G.J. Arendse, G.C. Hillhouse, J.V. Pilcher, F.D. Smit and R. Neveling, Phys. Rev. C 59, 2097 (1999).

[Tam81] T. Tamura, H. Lenske and T. Udagawa, Phy. Rev. C 23, 2769 (1981).

[Tra89] M. Trabandt, W. Scobel, M. Blann, B.A. Pohl, R.C. Byrd, C.C. Foster, R. Bonetti, Phys. Rev. C 39, 452 (1989).

[Wan80] C. W. Wang, N. S. Chant, P. G. Roos, A. Nadasen, and T. A. Carey, Phys. Rev. C21, 1705 (1980).

[Wan85] C. W. Wang, P.G. Roos, N.S. Chant, G. Ciangaru, F. Khazaie and D.J. Mack, Phys. Rev. C 31, 1662 (1985).

[Wol52] P.A. Wolff, Phys. Rev. C 87, 434 (1952).

[Wu79] J.R. Wu, C.C. Chang and H.D. Holmgren, Phys. Rev. C 19, 689 (1979)

[Yod94] N. R. Yoder, IUCF VME Data acquisition System User Information Manual, Indiana University Cyclotron Facility (1994).

[Yos98] T. Yoshimura , A. Okihana, R.E.Warner, N.S. Chant, P.G. Roos, C. Samanta, S. Kakigi, M. Fujiwara, N. Matsuoka, K. Tamura, E. Kubo and K. Ushiro, Nucl. Phys, A 641 (1998)